The Study on Neutralization of Human Immunodeficiency Virus and SARS CoV-2

– Neutralization Resistance of SHIV and Neutralization Assay for SARS CoV-2 –

YALCIN PISIL

Contents

摘要

後天性免疫不全症候群（AIDS）を引き起こすヒト免疫不全ウイルス（HIV）は、1981年に最初に認識され、世界的に流行した。国連エイズプログラムによると推定 7,570 万人が感染し、3,270 万人が死亡している。一方、新型コロナウイルス感染症(COVID-19)の原因ウイルスである SARS コロナウイル 2 型(SARS-CoV-2)は、2019 年に認識され、世界的大流行を起こした。世界保健機関によると 1 億人以上に影響を及ぼし、200 万人以上が死亡した。AIDS と COVID-19 に対するワクチンと治療薬の開発が望まれているが、そのためには感染症における防御免疫として中心的な働きをする中和抗体について理解することが重要である。

そこで、第 1 章では、中和抗体について概要を説明した。中和抗体による感染防御機構は、ウイルス感染メカニズムにも関係し、その活性を測定する方法は、ワクチン候補や新たな抗ウイルス薬候補を迅速に評価することに役立つ。

第 2 章では、サル／ヒト免疫不全ウイルス（SHIV）の中和抵抗性について調べた。中和感受性および抵抗性 SHIV の遺伝情報に基づき、中和感受性 SHIV の外皮タンパク遺伝子(*env*)にアミノ酸置換を導入し、中和抵抗性を詳細に比較解析した。その結果、中和抵抗性獲得に重要な変異が *env* の立体構造変化に関与することが示唆された。

第 3 章では、HIV のシュードタイプウイルスを用いた中和測定系に SARS-CoV-2 の外被タンパク遺伝子を組み合わせて、SARS-CoV-2 に対する中和抗体を評価するより効率的かつ安全な中和活性測定法を開発した。

本研究で得られた知見は、今後のHIVおよびSARS-CoV-2のワクチン開発や新規治療法開発に役立つものと期待される。

Summary

Human immunodeficiency virus (HIV) is a global pandemic, according to the United Nations program on AIDS. SARS-CoV-2 has affected about 100 million people and killed more than 2 million as a worldwide pandemic, according to the World Health Organization.

All attention for HIV and SARS-CoV-2 has focused on the development of vaccines and new antiviral agents. The process the developing antiviral drugs or vaccine candidates need long times even years from the discovery of drug or vaccine candidates to their launch by safety and efficiency. However, neutralizing monoclonal antibodies (NmAb) have been isolated from HIV infected patients and SARS-CoV-2 infected people with recombinant monoclonal antibody techniques. Passive administration of NmAbs could be protective against pathogen viruses such as HIV and SARS-CoV-2. NAb is a useful tool for understanding the mechanism of viral infection and evaluating new antiviral agent candidates. In chapter 1, I explained neutralizing antibodies by an overview.

Chapter 2 investigates the mechanism of neutralization resistance in a tier 2 SHIV clone, specifically the amino acid substitutions that make it tier 1 SHIV resistant. I introduced amino acid substitutions into the tier 1 SHIV env gene by in vitro mutagenesis based on the amino acid

alignment of the tier 1 SHIV and tier 2 SHIV virus strains, and then compared their neutralization resistance.

NAbs provide the potential for life saving therapies against SARS-CoV-2 either directly or indirectly (convalescent plasma) as well as a therapeutic and prophylactic treatment. NAb is a useful tool for understanding the mechanism of viral infection, and evaluating new antiviral agent candidates. Chapter 3 discusses a novel neutralization assay method-based modified cell system, which will be used to evaluate new antiviral drug targets against the epitopes on the SARS-CoV-2 spike protein and study the mechanism of binding to the host cell receptor.

The findings obtained in this study are expected to be useful for the future development of HIV and SARS-CoV-2 vaccines and new treatments.

Chapter 1.

Neutralizing Antibodies: An Overview

1.1. Structure and Isotypes of Immunoglobulins

An Immunoglobulin (Ig), also known as an antibody (Ab), is a large Y-shaped protein synthesized by white blood cells in response to antigenic stimulation [1]. The basic Ig has Y-shaped heterodimeric glycoproteins [1, 2] and is composed of two light and two heavy chains covalently bound via disulfide bridges (figure 1).

There are five classes or isotypes of heavy chains—γ, α, μ, δ, and ε—corresponding to the heavy chains of IgG, IgA, IgM, IgD, and IgE, respectively (Figure 1). There are two types of light chains in humans—κ and λ [3]. Each component chain contains one NH2-terminal "variable" domain and one or more COOH-terminal "constant" domains (Figure 1). These domains consist of two sandwiched β pleated sheets pinned together by a disulfide bridge between two conserved cysteine residues [2] (Figure 1). The Variable domain is distinguished by different amino acid sequences in the constant domain [3]. The heavy chain constant domains can be switched to allow altered effector function while maintaining antigen specificity [2].

Antibodies are arranged into three fragments that roughly form the shape of a Y. Two are antigen-binding fragments called Fab (F = fragment, ab = binding to antigen) (Figure 1). These binding regions are very flexible, allowing the antibody to bind easily to an antigen containing multiple binding sites without covalent interaction. Weak forces including electrostatic

interactions, hydrogen bonding, hydrophobic interactions, and van der Waals forces stabilize binding [4] [5, 6]. The third fragment is called the Fc (fragment crystallizable) region, which forms the trunk of the Y shape (Figure 1). The Fc region interacts with effector cells via their Fc receptors (FcR) and some proteins of the complement system, leading to activation of the immune system [4] [5]

Immunoglobulin G (IgG) is the most abundant antibody found in serum and the predominant isotype found in the body. IgG antibodies contribute directly to an immune response to identify and neutralize foreign toxins and viruses. IgG can be split into four subclasses: IgG1, IgG2, IgG3, and IgG4, each with its own biologic properties (e.g. complement activation and Fc receptor binding) [2] [7]. IgM is the first immunoglobulin expressed during B-cell development [2]. IgM is a high molecular weight protein (macroglobulin), consisting of five to six subunits (IgM monomers) (Figure 1). A pentameric IgM molecule has 10-antigen combining sites and can bind 10 small antigens (haptens). However, due to steric restrictions, only five large antigen molecules can be bound by one IgM molecule [8].

IgA is critical for protecting mucosal surfaces from toxins, virus and bacteria through either direct neutralization or by blocking binding to the mucosal surface [2]. In the blood, IgA represents about 10-15% of serum Ig in humans (versus 65%-75% IgG) and has a shorter half-life than IgG. The predominant form of IgA in human serum or plasma is monomeric, but there are small quantities of dimers, and fewer still trimers and tetramers [9]. The main molecular form found at mucosal surfaces, known as secretory IgA, is dimeric [10] (Figure1). IgA can be split into IgA1 and IgA2. IgA serum levels are considerably lower than IgG but tend to be higher than IgM. Conversely, IgA is the predominant isotype at mucosal surfaces and in secretions, including saliva and breast milk.

Though IgE is present at the lowest serum concentration with the shortest half-life, it is a very potent immunoglobulin. It is associated with hypersensitivity and allergic reactions as well as the response to parasitic worm infections [2] [9]. The function of circulating IgD is unclear, as it is not known to participate in the major antibody effector mechanisms [2].

1.2. The Functions of Antibodies

Generally, there are three functions of antibodies.

1) Neutralization: Neutralizing antibodies are secreted into the blood and mucosa where they bind to and block the infectivity or pathogens such as viruses, bacteria, parasites, and fungi [11].

2) To activate the complement system, a complementary pathway that induces a series of inflammatory responses that help to fight infection [6].

3) Opsonization: Antibodies facilitate the destruction of pathogens by phagocytic cells. Phagocytes include granulocytes (i.e. neutrophils, eosinophils, basophils, and mast cells), monocytes/macrophages and dendritic cells [12]. Opsonization begins when a pathogen is marked with an Fc-mediated antibody binding. Tagged pathogens are then eliminated via FcRs expressed on innate immune effectors cells such as monocytes/macrophages, neutrophils, dendritic cells and natural killer (NK) cells [13]. Two important opsonization mechanisms are Antibody-Dependent Cellular Cytotoxicity (ADCC) and Antibody-Dependent Cellular Phagocytosis (ADCP) [14]. ADCC is a mechanism of immune defense whereby an FcR-bearing effector cell can recognize and kill antibody-coated target cells expressing tumour- or pathogen-derived antigens on their surface [15]. ADCP is the mechanism by which antibody-coated target cells activate the FcRs on the surface of macrophages to induce phagocytosis, resulting in internalization and degradation of the target cell through phagosome acidification [14].

1.3. Polyclonal Antibodies

A B-lymphocyte will produce a single specific antibody against an antigen. Polyclonal antibodies are antibodies that are secreted by many different B cell lineages against a specific antigen, generating antibody clones with varying structure [4, 16]. Polyclonal antibodies can be produced faster than monoclonal antibodies with lower cost, lower technical skill, and are stable over a broad range of pH and salt concentrations [17]. However, due to cross-reactivity of antibodies and the need for more controllable assays, it can be advantageous to have a homogeneous high affinity antibody preparation specific for a single epitope [4].

1.4. Monoclonal Antibodies

Monoclonal antibodies are synthesized from a single B-lymphocyte cell clone and are specific to a single epitope. In recent years, there has been a great need for high quality monoclonal antibodies in both research and clinical settings [1].

Monoclonal antibodies are an essential part of *in vitro* diagnostics technology such as radioimmunoassays, enzyme-linked immunosorbent assays, immunocytopathology and flow cytometry. They are an exciting tool for *in vivo* clinical diagnostics and cancer immunotherapy [18]. The first monoclonal antibody to be approved for use was OKT3 (target T cell CD3 receptor) and is an immunosuppressant drug used in organ transplantation [18].

1.4.1. Producing Monoclonal Antibodies

During B cell development, the gene segments encoding the heavy and light chains undergo random genetic recombination (V(D)J recombination). This leads to mature B cells producing antibodies with a unique amino acid sequence in the antigen-binding region [19]. Antibody repertoire diversity can be as high as 10^{11} unique molecules in a single individual, with every B cell producing an antibody with a unique antigen specification [19]. This diverse repertoire confounds characterization by conventional sequence analyses [20]. B cells, also known as antigen-presenting cells (APCs), are responsible for the humoral immune response. Most B lymphocytes are found in the cortex of lymph nodes, follicles in Peyer's plaques, bone marrow, follicles of the spleen, and the marginal zone of the white pulp. Few lymphocytes in the peripheral blood are B cells [21].

B cell and T cell activation occur in the interfollicular region of the spleen or lymph node. T cell receptor (TCR)-mediated recognition of an antigen displayed on MHC II leads to the expression of CD40 ligand (CD40L) and secretion of interleukin 21 (IL-21) by T follicular helper cells. Engagement of CD40 (expressed by B cell) with CD40L (expressed by T cell) stimulates B cell survival, proliferation (clonal expansion) and differentiation. CD40L-mediated signals combined with cytokines secreted by TFH cells (IL-21, IL-10, IL-4) enhance B cell proliferation and can induce CSR (class-switch recombination) [22]. Defects occurring through somatic

hypermutation (SHM) may result in the formation of B cells, which bind with high affinity to self-antigens [21]. SHM and CSR are necessary for antibody diversification in antigen-specific memory B cells [23]. After a first encounter of the antigen by vaccination or natural infection, immunological memory allows for more rapid production of neutralizing antibodies following the next exposure to the virus [6].

1.4.2. Neutralizing Antibodies

Neutralizing antibodies (nAb) derived from B cells are part of the humoral response of the adaptive immune system. Immunity due to neutralizing antibodies is also known as sterilizing immunity. Sterilizing immunity is a unique immune status that prevents effective viral infection in the host [24]. NAb are often confused with binding antibodies. While binding antibodies are targeting pathogens for disposal by the immune system, nAbs directly inactivate a pathogen by directly inhibiting its ability to infect host cells. [25, 26].

Effective vaccines stimulate the production of neutralizing antibodies against a target antigen [27]. Once the acute infection has cleared, circulating nAbs provide long term resistance against re-infection. But vaccine candidates against some major viral pathogens, including HIV-1, have failed to induce a potent and effective response [25]. Merck's adenovirus type 5 (Ad5)-based HIV-1 vaccine program was announced in 2004 and stopped abruptly in 2007. While the vaccine candidate had a protective effect in a non-human primate model it was unable to produce neutralizing antibodies against HIV in the human clinical trials [28-30]. The RV 144 HIV Vaccine program was sponsored by the Surgeon General from September 2003 until December 2005 and produced only a modest benefit [31].

NAb can inhibit viral infection at one of four stages, which occur during the attachment and entry portion of the viral replicative cycle. 1) NAb binds to viral receptor-binding protein and

blocks viral docking onto the receptor on the cell surface [25]. 2) Once the virus has docked, NAb binds to an epitope on the envelope glycoprotein. This inhibits virus and host cell interactions, such as the fusogenic refolding of the viral envelope glycoprotein to interact with a second receptor (CXCR4/CCR5 of HIV) on the cell surface [25, 32]. 3) Virion has already started to fuse with the cell membrane. NAbs bind to membrane-proximal epitopes of the virus and inhibit the membrane fusion step of viral entry [25]. 4) Post-entry neutralization, where nAbs remain attached to viruses after cell infection and initiate an intracellular immune response [25].

1.4.2.1. The Neutralization Category of Virus.

Neutralizing antibodies can lose their binding specificity over time due to the high degree of sequence variability and structural plasticity in target viral epitopes, such as the HIV trimeric envelope glycoproteins (Env) [33]. Pseudo viruses are categorized by their interaction with NAbs and the IgG fractions of serum from HIV-1 infected individuals. Tier 1 A and B viruses are easily neutralized by HIV-1 infected human pooled plasma and representative laboratory strain (existing SHIV). Tier 1 A is more sensitive than 1B. Tier 2 viruses are more difficult to neutralize and represent general HIV-1 clinical strains. Tier 3 viruses are very difficult to neutralize [33, 34].

1.4.2.2. Neutralizing Antibody Assays

Bioluminescent organisms generate light by the creation of an excited-state reaction product, which then decays to its ground state and emits a photon. The most efficient bioluminescent reaction known is that of the firefly. The firefly bioluminescence reaction emits light via a chemical reaction that converts luciferin to oxyluciferin by the luciferase enzyme [35].

Luciferase is a popular reporter gene, as the sensitivity and linear response range are superior to other typical reporter genes such as β-galactosidase, chloramphenicol acetyltransferase, β-glucuronidase and green fluorescent protein. Luciferases reporter genes are used for quantitative measurement of gene expression [36] and protein expression [37]. Luciferase activity is quantified by relative illumination/light units (RLU), and is directly proportional to the number of infectious virus particles found in the first inoculum over a wide range of values [38].

NAb assays are potent tools for assessing humoral immunity in HIV-1 viral infections and examining candidate vaccine immunogens in preclinical and clinical trials [38, 39]. NAb assays were first conducted for HIV-1 using based TZM-bl cells by Dr. George Shaw and his colleagues [40, 41]. TZM-bl indicator cell line (also called JC.53bl-13) is a HeLa cell derivative that was further engineered to contain Tat-responsive reporter genes for either β-gal or firefly luciferase to quantitate the infection of HIV-based vectors (Figure 2). These engineered features made TZM-bl cells highly susceptible to HIV-1 infection and become a readily quantifiable assay to titrate neutralizing Abs [42]. TZM-bl cells are genetically modified and selected to express CD4+, CCR5+ and CXCR4+ constitutively [41] (Figure 2). This makes TZM-b1 cells susceptible to infection by a wide variety of HIV, SIV and SHIV strains, including primary HIV isolates and molecularly cloned Env-pseudotyped viruses [38, 43] (Figure 2). TZM-bl cells are maximally sensitive to HIV infection in DEAE-dextran (Deax) including medium [42] [41, 43].

Neutralization assays were performed in 96-well plates for high throughput capacity. The 50% inhibitory concentration (IC50) or dose (ID50) were reported as either the concentration for purified reagents (for IC50) or serologic reagent dilution (for ID50) at which RLU were reduced by 50% compared to background RLU in virus control wells (cells + virus without test sample) after subtraction of background RLU from cell control wells (cells only) [42, 44].

N mAbs have great potential in both therapeutic and prophylactic applications against viral pathogens such as HIV-1 and SARS-CoV-2. NAb assays provide a useful tool to understand infectivity mechanism of viral pathogenesis and to evaluate new antiviral candidates rapidly. For these reasons, the N mAb assay is used in the experimental designs of Chapter 2 and Chapter 3 (Figure 2).

1.4.2.3. Human antibodies that neutralize HIV-1

Antiretroviral agents suppress HIV-1 replication and have been used clinically to treat HIV-1 infection in patients. However, completely eliminating latent HIV-1 is very difficult. Suppression and prevention of HIV-1 replication by passive administration of neutralizing antibodies (nAbs) could have beneficial therapeutic effects. Understanding the structure of the native HIV-1 envelope spike protein is critical for the development of successful vaccines and antiviral therapies [45].

HIV infection begins when the HIV envelope (Env) glycoprotein trimer binds to the primary cellular receptor CD4 and then to a cellular coreceptor (CCR5 or CXCR4) on the surface of host cells [46]. While 10–25% of those infected with HIV-1 can make antibodies that cross-neutralize many of the HIV-1 strains tested, only 1% have broad and potent nAb activity against HIV-1 [47] [48].

The isolation and characterization of neutralizing monoclonal antibodies has been an ongoing challenge [32]. Antibody V(D)J sequences in IgG heavy and light kappa/lambda chains have been successfully isolated from HIV infected human plasma or SIV infected rhesus macaque monkeys using single B cell cloning, hybridoma generation and phage display [49-56].

There are various mAb clones that specifically target common viral epitopes such as gp41 MPER (mAb 2F5, 4E10, 10e8), V1+V2 Region (mAb PG9, CAP 256(VRC26.25), PDGM1400), V3 Glycan region (mAb PGT121 and KD247) and the CD4 binding region (mAb 2G12, VRC01,VRC07-523, N6, 3BNC117) [22] [32] [57] [78] (Figure 3).

Whilst broad neutralizing antibodies (bNAbs) dock the same outer domain site of CD4 gp120, lower breadth mAb bind to different regions of the CD4-binding site [32]. While bNAbs such as VRC01, NIH45–46, 12A12, 3BNC117, VRC-PG04 and VRC-CH31 could neutralize 80%–90% of common viruses, lower breadth mAb such as b12, F105 and b13 only neutralize 40%, 10%, and 10%, respectively [32].

1.4.2.4. Neutralizing Antibodies against SARS-CoV-2

SARS-CoV-2 is a global pandemic that has killed more than 1.2 million and affected over 51 million people worldwide. The incubation time for SARS-CoV-2 is relatively long and lasts between 2–14 days. Increased IgM and IgA are the early antibody response that peaks within 7 days, with specific IgG antibodies developing 10 to 18 days post infection. These IgGs are assumed to continue lifelong as protective antibodies [58]. The majority of serological tests focus on IgM and IgG, although IgA is the main isotype involved in mucosal immunity [58]. There is not yet any antiviral drug or vaccine against SARS-CoV-2 due to a limited knowledge about SARS-CoV-2 and the time it takes from generation of a drug/vaccine to its launch [59, 60]. Current clinical management of COVID-19 includes infection prevention, control measures and supportive care, including supplemental oxygen and mechanical ventilatory support when indicated. The U.S. Food and Drug Administration (FDA) has approved one drug, remdesivir (Veklury), for the treatment of COVID-19 in certain situations.

Convalescent plasma from patients who have recovered from SARS-CoV2 is also used widely against Covid-19 [60]. Newly infected patients are treated with convalescent plasma infusions to transfer antibodies generated by people who have previously recovered from Covid-19 [61]. Plasma therapy runs the risk of allergic/anaphylactic reactions, white blood cell/red blood cell alloimmunization, lung damage and difficulty breathing, hemolytic transfusion reactions and infections such as HIV, hepatitis B and hepatitis C [62]. Convalescent plasma has lower levels of virus-neutralizing antibodies compared to concentrated and purified mAb and has limited antiviral therapy efficiency. A ten-fold dilution of convalescent plasma has no protective effect against SARS-CoV-2 [63]. However, passive administration of mAbs is a promising solution to the spread of SARS-CoV-2 and may help with the development of vaccines and drug candidate discovery [64]. Additionally, mAb may be more effective and safe than convalescent plasma for treating COVID-19 [62] [63].

The receptor-binding domain (RBD) on the S protein of SARS-CoV-2 uses angiotensin-converting enzyme 2 (ACE2) as its receptor for cell entry, which initiates the infection process [65-67] (figure4). When the S protein binds to the receptor, TM protease serine 2 (TMPRSS2), a type 2 TM serine protease located on the host cell membrane, further cleaves the S2 subunit of S protein into S2' and S2" subunits activating the membrane fusion domain [68]. The RBD is a major target for antibodies such as 47D11,S309, 206 and BD-368-2 [64, 70-72] (Figure 4)

In a recent study, 90% of mild-to-moderate SARS-CoV-2 infected individuals had robust plasma IgG antibody responses and these Ab titers remain stable for 5 months after infection [69]. The 206 RBD-specific monoclonal antibodies derived from single B cells of infected individuals neutralized 98–99% of pseudo-typed lentiviral SARS-CoV-2/spike and live SARS-CoV-2 proteins [70]. In addition, 14 potent SARS-CoV-2 neutralizing antibodies were found in a B cell sorting

isolated from 60 convalescent patients. The RBD-specific mAb BD-368-2 from these nAbs showed high therapeutic and prophylactic efficacy in SARS-CoV-2-infected mice [71]. The 47D11 antibody targets a conserved RBD epitope (residues 338–506) in the SARS2-S-S1B domain and binds to recombinant full-length spike proteins of SARS-CoV and SARS-CoV-2 [72]. The 47D11 antibody could potently inhibit a pseudo-typed VSV / SARS-Spike and pseudo-typed VSV / SARS2-spike infection in VeroE6 cells [72]. Combining several nAb clones can have a synergetic effect on neutralizing SarsCov2 by recognizing different epitopes on the receptor-binding domain [73].

Several monoclonal antibodies that target the S glycoprotein of SARS-CoV, such as the S309 Ab identified from memory B cells of a SARS-CoV infected individual [64], could be repurposed to target the same epitope on SARS-CoV-2 . The electrostatic potential of viral protein structure could also impact infectivity. In a study that highlighted the importance of particle charge on infectivity, mouse hepatitis coronavirus A59 viral particles could not be isolated when negatively charged residues were replaced by positively charged amino acids [74]. Another study reported that, despite the structural and functional similarity of the S proteins of SARS-CoV-2 and SARS-CoV, the former has a higher infectivity rate and has a slightly more positive charge. Positively charged residues may lead to increased binding affinity toward negatively charged regions of host receptor molecules. Analysis of the S protein binding to host ACE2 receptor showed a 30% higher binding energy for SARS-CoV-2 than for the SARS-CoV S protein [75]. Another report demonstrated that D614G substitution enhances SARS-CoV-2 infectivity [76]. There is speculation that the positive charge electrostatic potential of the spike protein might increase binding ability against the negatively charged region of the ACE2 receptor [75] [76].

1.5. Conclusion

NAbs were secreted against various epitopes on the surface unit (gp120) and the transmembrane unit (gp41) of the HIV envelope glycoprotein (Env) as well as against epitopes occurring on the 3-D structure of trimeric Env spike protein [32]. Recently, progress has been made in identifying and characterizing highly potent broadly neutralizing antibodies for HIV-1 therapy and vaccine design. However, HIV-1 exhibits genetically diverse populations due to rapid viral evolution. This commonly leads to drug resistance and/or immune evasion, and is a significant barrier to the development of an effective HIV-1 treatment [77].

Chapter 2 investigates the mechanism of neutralization resistance in a tier 2 SHIV clone, specifically the amino acid substitutions that make it tier 1 SHIV resistant. I introduced amino acid substitutions into the tier 1 SHIV env gene by in vitro mutagenesis based on the amino acid alignment of the tier 1 SHIV and tier 2 SHIV virus strains, and then compared their neutralization resistance.

NAbs provide the potential for life saving therapies against SARS-CoV-2 either directly or indirectly (convalescent plasma) as well as a therapeutic and prophylactic treatment. NAb is a useful tool for understanding the mechanism of viral infection, and evaluating new antiviral agent candidates. Chapter 3 discusses a novel neutralization assay method-based modified cell system,

which will be used to evaluate new antiviral drug targets against the epitopes on the SARS-CoV-2 spike protein and study the mechanism of binding to the host cell receptor.

1.6. Reference

1. Abbas, A.K., A.H. Lichtman, and S. Pillai, *Cellular and molecular immunology*. 2010: Philadelphia, PA : Saunders/Elsevier, c2010.
2. Schroeder, H.W., Jr. and L. Cavacini, *Structure and function of immunoglobulins.* J Allergy Clin Immunol, 2010. 125(2 Suppl 2): p. S41-52.
3. Actor, J.K., *Chapter 3 - Humoral Immunity: Antibody Recognition of Antigen*. Immunology and Microbiology (Second Edition), . 2012: Saunders.
4. K.Actor, J., *Chapter 12 - Assessment of Immune Parameters and Immunodiagnostics*. Introductory Immunology, Basic Concepts for Interdisciplinary Applications. 2014: Academic Press.
5. Feldkamp, C.S. and J.L. Carey, *2 - IMMUNE FUNCTION AND ANTIBODY STRUCTURE*, in *Immunoassay*, E.P. Diamandis and T.K. Christopoulos, Editors. 1996, Academic Press: San Diego. p. 5-24.
6. Janeway, C.A., et al., *Janeway's immunobiology*. Vol. pbk. 2012: Garland Science.
7. Paul, W.E., *Fundamental immunology*. 2008, Philadelphia: Wolters Kluwer/Lippincott Williams & Wilkins.

8. Nezlin, R., *CHAPTER 1 - General Characteristics of Immunoglobulin Molecules*, in *The Immunoglobulins*, R. Nezlin, Editor. 1998, Academic Press: New York. p. 3-73.

9. Li, M., et al., *Human immunodeficiency virus type 1 env clones from acute and early subtype B infections for standardized assessments of vaccine-elicited neutralizing antibodies.* J Virol, 2005. 79(16): p. 10108-10125.

10. de Sousa-Pereira, P. and J.M. Woof, *IgA: Structure, Function, and Developability.* Antibodies (Basel), 2019. 8(4).

11. Forthal, D.N., *Functions of Antibodies.* Microbiology spectrum, 2014. 2(4): p. 1-17.

12. Anaya, J.M., et al., *Autoimmunity: From Bench to Bedside*, in *Autoimmunity: From Bench to Bedside*, J.M. Anaya, et al., Editors. 2013, El Rosario University Press© 2013 Universidad del Rosario.: Bogota (Colombia).

13. Duchemin, M., et al., *Antibody-Dependent Cellular Phagocytosis of HIV-1-Infected Cells Is Efficiently Triggered by IgA Targeting HIV-1 Envelope Subunit gp41.* Front Immunol, 2020. 11: p. 1141.

14. Tay, M.Z., K. Wiehe, and J. Pollara, *Antibody-Dependent Cellular Phagocytosis in Antiviral Immune Responses.* Front Immunol, 2019. 10: p. 332.

15. Gómez Román, V.R., J.C. Murray, and L.M. Weiner, *Chapter 1 - Antibody-Dependent Cellular Cytotoxicity (ADCC)*, in *Antibody Fc*, M.E. Ackerman and F. Nimmerjahn, Editors. 2014, Academic Press: Boston. p. 1-27.

16. Sabeta, C. and E. Ngoepe, *Chapter Seven - Preparation of Fluorescent Antibody Conjugate in Goats*, in *Current Laboratory Techniques in Rabies Diagnosis, Research and Prevention, Volume 2*, C. Rupprecht and T. Nagarajan, Editors. 2015, Academic Press. p. 69-81.

17. Saeed, A.F., et al., *Antibody Engineering for Pursuing a Healthier Future.* Front Microbiol, 2017. 8: p. 495.

18. Waldmann, T.A., *< THOMAS A. WALDMANN1991,Monoclonal Antibodies in Diagnosis and Therapy.pdf>.* 1991.

19. Jung, D. and F.W. Alt, *Unraveling V(D)J Recombination: Insights into Gene Regulation.* Cell, 2004. 116(2): p. 299-311.

20. Glanville, J., et al., *Precise determination of the diversity of a combinatorial antibody library gives insight into the human immunoglobulin repertoire.* Proc Natl Acad Sci U S A, 2009. 106(48): p. 20216-20221.

21. Özbek, M., *B Cell Development.* MAKÜ Sag. Bil. Enst. Derg., 2016. 4(2): 88-95.

22. Budzyńska, P.M., *REGULATION_OF_B CELL DEVELOPMENT BY TRANSCRIPTION*, T. University, Editor. 2017: TURUN YLIOPISTON JULKAISUJA – ANNALES UNIVERSITATIS TURKUENSIS.

23. Izumi, T. and I. Mellon, *Chapter 17 - Base Excision Repair and Nucleotide Excision Repair*, in *Genome Stability*, I. Kovalchuk and O. Kovalchuk, Editors. 2016, Academic Press: Boston. p. 275-302.

24. Dutta, A., et al., *Sterilizing immunity to influenza virus infection requires local antigen-specific T cell response in the lungs.* Sci Rep, 2016. 6: p. 32973.

25. Klasse, P.J., *Neutralization of Virus Infectivity by Antibodies: Old Problems in New Perspectives.* Adv Biol, 2014. 2014.

26. Zoppi, L., *<zoppi,2020,What-are-Neutralizing-Antibodies.pdf>.* 2020.

27. Koff, W.C., et al., *Accelerating next-generation vaccine development for global disease prevention.* Science, 2013. 340(6136): p. 1232910.

28. Anonymous, *HIV vaccine failure prompts Merck to halt trial.* Nature, 2007. 449(7161): p. 390-390.

29. Watkins, D.I., et al., *Nonhuman primate models and the failure of the Merck HIV-1 vaccine in humans.* Nat Med, 2008. 14(6): p. 617-621.

30. Miura, Y.I.a.T., *Nonhuman Primate Models for Empirical Research of Acquired Immunodeficiency Syndrome.* Annals of Virology and Research, 2016. 2(2):1016.

31. Rerks-Ngarm, S., et al., *Vaccination with ALVAC and AIDSVAX to Prevent HIV-1 Infection in Thailand.* New England Journal of Medicine, 2009. 361(23): p. 2209-2220.

32. Kwong, P.D. and J.R. Mascola, *Human antibodies that neutralize HIV-1: identification, structures, and B cell ontogenies.* Immunity, 2012. 37(3): p. 412-425.

33. Montefiori, D.C., et al., *Neutralization tiers of HIV-1.* Curr Opin HIV AIDS, 2018. 13(2): p. 128-136.

34. Seaman, M.S., et al., *Tiered categorization of a diverse panel of HIV-1 Env pseudoviruses for assessment of neutralizing antibodies.* J Virol, 2010. 84(3): p. 1439-1452.

35. Milne, B.F., M.A. Marques, and F. Nogueira, *Fragment molecular orbital investigation of the role of AMP protonation in firefly luciferase pH-sensitivity.* Phys Chem Chem Phys, 2010. 12(42): p. 14285-14293.

36. Nakajima, Y., et al., *Multicolor luciferase assay system: one-step monitoring of multiple gene expressions with a single substrate.* Biotechniques, 2005. 38(6): p. 891-894.

37. Carter, M. and J. Shieh, *Chapter 15 - Biochemical Assays and Intracellular Signaling*, in *Guide to Research Techniques in Neuroscience (Second Edition)*, M. Carter and J. Shieh, Editors. 2015, Academic Press: San Diego. p. 311-343.

38. Montefiori, D.C., *Measuring HIV neutralization in a luciferase reporter gene assay.* Methods Mol Biol, 2009. 485: p. 395-405.

39. Montefiori, D.C., *Evaluating neutralizing antibodies against HIV, SIV, and SHIV in luciferase reporter gene assays.* Curr Protoc Immunol, 2005. Chapter 12: p. Unit 12.11.

40. Wei, X., et al., *Emergence of resistant human immunodeficiency virus type 1 in patients receiving fusion inhibitor (T-20) monotherapy.* Antimicrob Agents Chemother, 2002. 46(6): p. 1896-1905.

41. Wei, X., et al., *Antibody neutralization and escape by HIV-1.* Nature, 2003. 422(6929): p. 307-312.

42. Sarzotti-Kelsoe, M., et al., *Optimization and validation of a neutralizing antibody assay for HIV-1 in A3R5 cells.* J Immunol Methods, 2014. 409: p. 147-160.

43. Pisil, Y., et al., *Specific Substitutions in Region V2 of gp120 env confer SHIV Neutralisation Resistance.* Pathogens, 2020. 9(3).

44. Platt, E.J., et al., *Evidence that Ecotropic Murine Leukemia Virus Contamination in TZM-bl Cells Does Not Affect the Outcome of Neutralizing Antibody Assays with Human Immunodeficiency Virus Type 1.* Journal of Virology, 2009. 83(16): p. 8289-8292.

45. Munro, J.B. and W. Mothes, *The HIV-1 Env trimer in HD.* Structure, 2014. 22(7): p. 935-936.

46. Wilen, C.B., J.C. Tilton, and R.W. Doms, *HIV: cell binding and entry.* Cold Spring Harb Perspect Med, 2012. 2(8).

47. Hraber, P., et al., *Prevalence of broadly neutralizing antibody responses during chronic HIV-1 infection.* AIDS, 2014. 28(2): p. 163-169.

48. Simek, M.D., et al., *Human immunodeficiency virus type 1 elite neutralizers: individuals with broad and potent neutralizing activity identified by using a high-throughput neutralization assay together with an analytical selection algorithm.* J Virol, 2009. 83(14): p. 7337-7348.

49. Arts, E.J. and D.J. Hazuda, *HIV-1 antiretroviral drug therapy.* Cold Spring Harb Perspect Med, 2012. 2(4): p. a007161.

50. Kuwata, T., et al., *Isolation of potent neutralizing monoclonal antibodies from an SIV-Infected rhesus macaque by phage display.* AIDS Res Hum Retroviruses, 2011. 27(5): p. 487-500.

51. N. Climent, H.O., F. García, C. Gil, S. Sánchez-Palomino, T. Pumarola, M. Plana, and J.A. J.M. Miró, J.M. Gatell, and T. Gallart, *Generation of Human Monoclonal Antibodies from HIV-Infected Individuals.* Inmunología, 2004. Vol. 23 / Núm 4/ Octubre-Diciembre 2004: 303-312.

52. Tiller, T., et al., *Efficient generation of monoclonal antibodies from single human B cells by single cell RT-PCR and expression vector cloning.* J Immunol Methods, 2008. 329(1-2): p. 112-124.

53. Wang, Z., et al., *Isolation of single HIV-1 Envelope specific B cells and antibody cloning from immunized rhesus macaques.* J Immunol Methods, 2020. 478: p. 112734.

54. Huang, J., et al., *Isolation of human monoclonal antibodies from peripheral blood B cells.* Nat Protoc, 2013. 8(10): p. 1907-1915.

55. Meng, W., et al., *Efficient generation of monoclonal antibodies from single rhesus macaque antibody secreting cells.* MAbs, 2015. 7(4): p. 707-718.

56. Babrak, L., et al., *Identification and verification of hybridoma-derived monoclonal antibody variable region sequences using recombinant DNA technology and mass spectrometry.* Molecular Immunology, 2017. 90: p. 287-294.

57. Ramirez Valdez, K.P., et al., *Complementary and synergistic activities of anti-V3, CD4bs and CD4i antibodies derived from a single individual can cover a wide range of HIV-1 strains.* Virology, 2015. 475: p. 187-203.

58. Nuccetelli, M., et al., *Combined anti-SARS-CoV-2 IgA, IgG, and IgM Detection as a Better Strategy to Prevent Second Infection Spreading Waves.* Immunol Invest, 2020: p. 1-13.

59. Gordon, D.E., et al., *A SARS-CoV-2 protein interaction map reveals targets for drug repurposing.* Nature, 2020. 583(7816): p. 459-468.

60. Marovich, M., J.R. Mascola, and M.S. Cohen, *Monoclonal Antibodies for Prevention and Treatment of COVID-19.* JAMA, 2020. 324(2): p. 131-132.

61. Liu, S.T.H., et al., *Convalescent plasma treatment of severe COVID-19: a propensity score-matched control study.* Nat Med, 2020.

62. Pandey, S. and G.N. Vyas, *Adverse effects of plasma transfusion.* Transfusion, 2012. 52 Suppl 1: p. 65S-79S.

63. Haagmans, B.L., et al., *SARS-CoV-2 neutralizing human antibodies protect against lower respiratory tract disease in a hamster model.* 2020.

64. Pinto, D., et al., *Cross-neutralization of SARS-CoV-2 by a human monoclonal SARS-CoV antibody.* Nature, 2020. 583(7815): p. 290-295.

65. Ren, W., et al., *Difference in Receptor Usage between Severe Acute Respiratory Syndrome (SARS) Coronavirus and SARS-Like Coronavirus of Bat Origin.* Journal of Virology, 2008. 82(4): p. 1899-1907.

66. Hoffmann, M., et al., *SARS-CoV-2 Cell Entry Depends on ACE2 and TMPRSS2 and Is Blocked by a Clinically Proven Protease Inhibitor.* Cell, 2020. 181(2): p. 271-280.e8.

67. Yang, R., et al., *Development and effectiveness of Pseudotyped SARS-CoV-2 system as determined by neutralizing efficiency and entry inhibition test in vitro.* Biosafety and Health, 2020.

68. Huang, Y., et al., *Structural and functional properties of SARS-CoV-2 spike protein: potential antivirus drug development for COVID-19.* Acta pharmacologica Sinica, 2020. 41(9): p. 1141-1149.

69. Wajnberg, A., et al., *Robust neutralizing antibodies to SARS-CoV-2 infection persist for months.* Science, 2020.

70. Ju, B., et al., *Potent human neutralizing antibodies elicited by SARS-CoV-2 infection.* publons.com/p/30909046/, 2020.

71. Cao, Y., et al., *Potent Neutralizing Antibodies against SARS-CoV-2 Identified by High-Throughput Single-Cell Sequencing of Convalescent Patients' B Cells.* Cell, 2020. 182(1): p. 73-84 e16.

72. Wang, C., et al., *A human monoclonal antibody blocking SARS-CoV-2 infection.* Nat Commun, 2020. 11(1): p. 2251.

73. ter Meulen, J., et al., *Human monoclonal antibody combination against SARS coronavirus: synergy and coverage of escape mutants.* PLoS Med, 2006. 3(7): p. e237.

74. Verma, S., et al., *Identification of functionally important negatively charged residues in the carboxy end of mouse hepatitis coronavirus A59 nucleocapsid protein.* J Virol, 2006. 80(9): p. 4344-4355.

75. Hassanzadeh, K., et al., *Considerations around the SARS-CoV-2 Spike Protein with Particular Attention to COVID-19 Brain Infection and Neurological Symptoms.* ACS Chem Neurosci, 2020. 11(15): p. 2361-2369.

76. Hou, Y.J., et al., *SARS-CoV-2 D614G variant exhibits efficient replication ex vivo and transmission in vivo.* Science, 2020: p. eabe8499.

77. Harada, S. and K. Yoshimura, *Driving HIV-1 into a Vulnerable Corner by Taking Advantage of Viral Adaptation and Evolution.* Front Microbiol, 2017. 8: p. 390.

78. Caskey, M., F. Klein, and M.C. Nussenzweig, *Broadly neutralizing anti-HIV-1 monoclonal antibodies in the clinic.* Nat Med, 2019. 25(4): p. 547-553.

1.7. Figures

Figure 1.

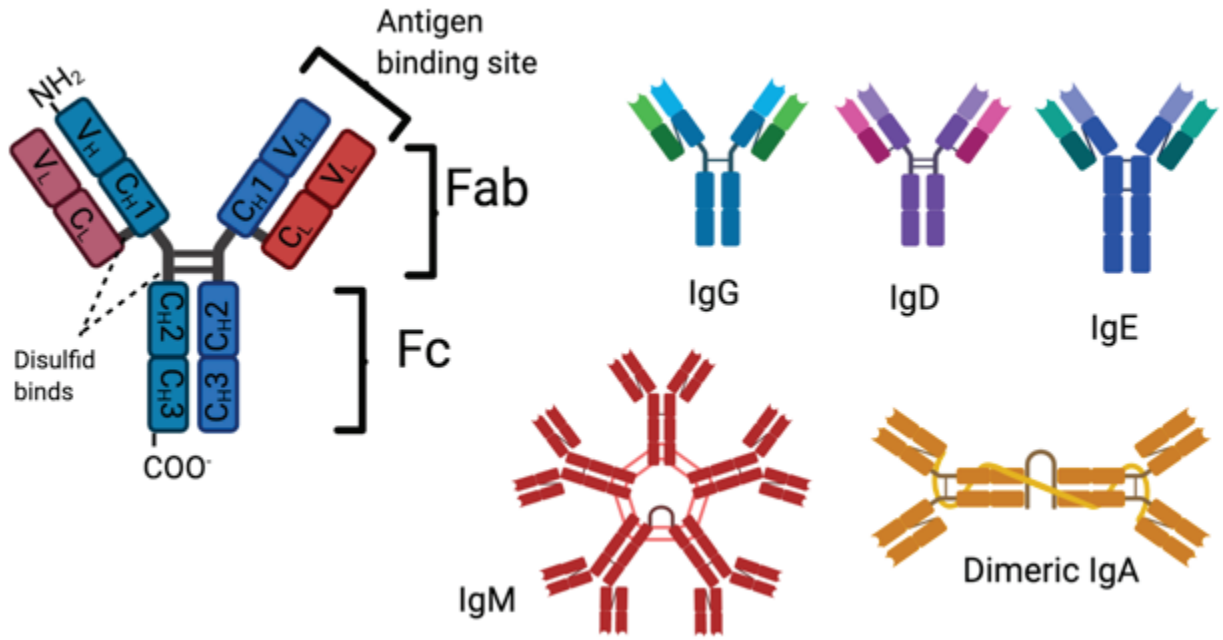

Structure and Isotypes of Immunoglobulins. The five classes of Ig: M, G, A, E, and D, distinguished by different heavy chains. Differences in the heavy chain constant domain between isotypes include the number and location of interchain disulfide bonds, the number of attached oligosaccharide moieties and the number of constant domains. V = Variable Domain, C = Constant Domain, H = Heavy Chain, L = Light Chain, Ig = Immunoglobin, F = fragment, ab = binding to antigen, Fc = fragment crystallizable region.

Figure 2.

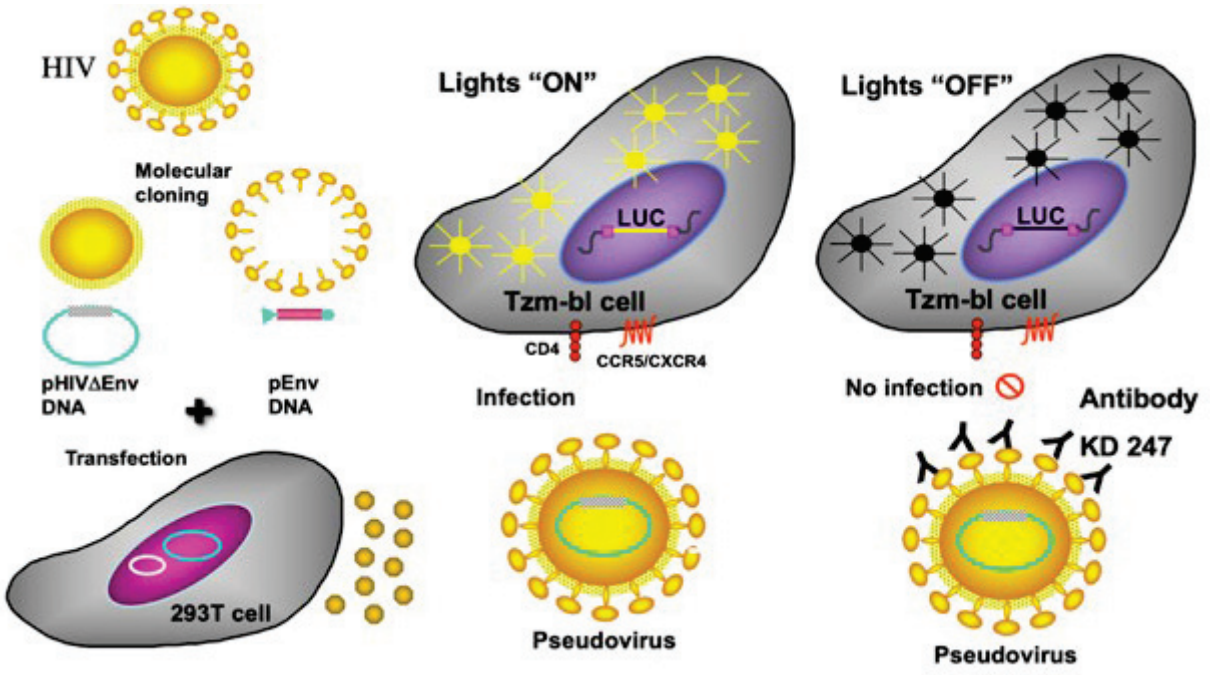

Sequential events in detecting neutralization of envelope pseudo-typed viruses in Tzm-bl cells**.** DNA plasmids were cloned by transforming into competent Stbl3 cells. Pseudo-type HIV viruses were constructed as described previously (Qu,2005). In brief, Pseudo-type HIV viruses harbouring HIV env plasmid were prepared by co-transfecting $5x10^5$ cell/ml 293T cells with pSGΔenv and pcDNA3.1 vectors expressing the respective env genes in the 200 µl OptiMem including 8 µl X-treme HP transfection reagent. Transfected 293 cell lines were incubated at 37ºC at 5% CO2. After 48 hours, supernatants (Pseudo-type HIV viruses) were harvested through 0.45 µm pore size filter (Millipore) and 400 µl stocks were made in 1.5 mL tubes and stored at -80ºC. TZM-bl (also called JC.53bl-13) is a HeLa cell derivative that was further engineered to contain Tat-responsive reporter genes for firefly luciferase (Luc) to quantitate the infection of HIV-based vectors. After a single cycle Pseudo-type HIV infection, luciferase reporter gene expression in TZM-bl Cell is stimulated in trans by the viral Tat protein. The expression of luciferase was examined about 2–3 days after the initial cell transfection.

Figure 3.

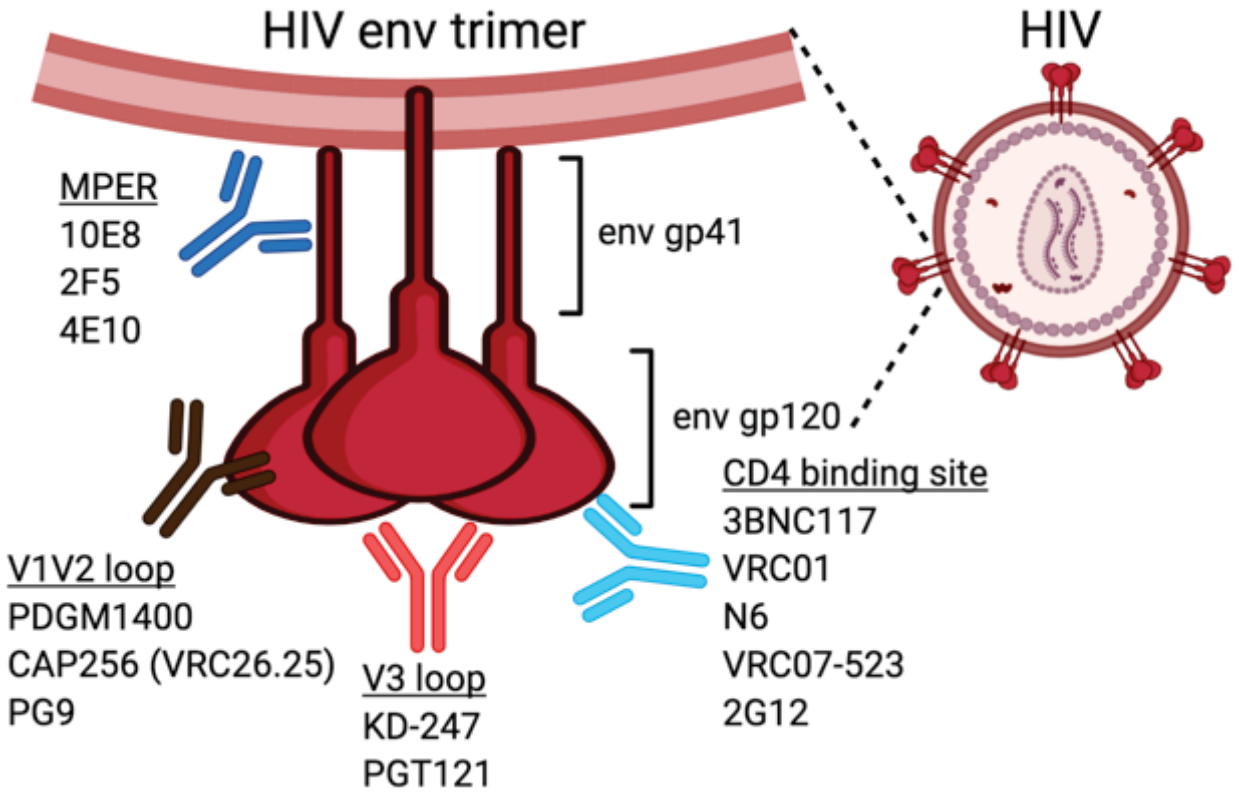

Neutralizing anti-HIV-1 monoclonal antibodies. Antibodies were categorized by their epitopes such as CD4bs (blue), the V1/V2 loop (brown), the V3-LOOP (red) and the MPER (navy).

Figure 4.

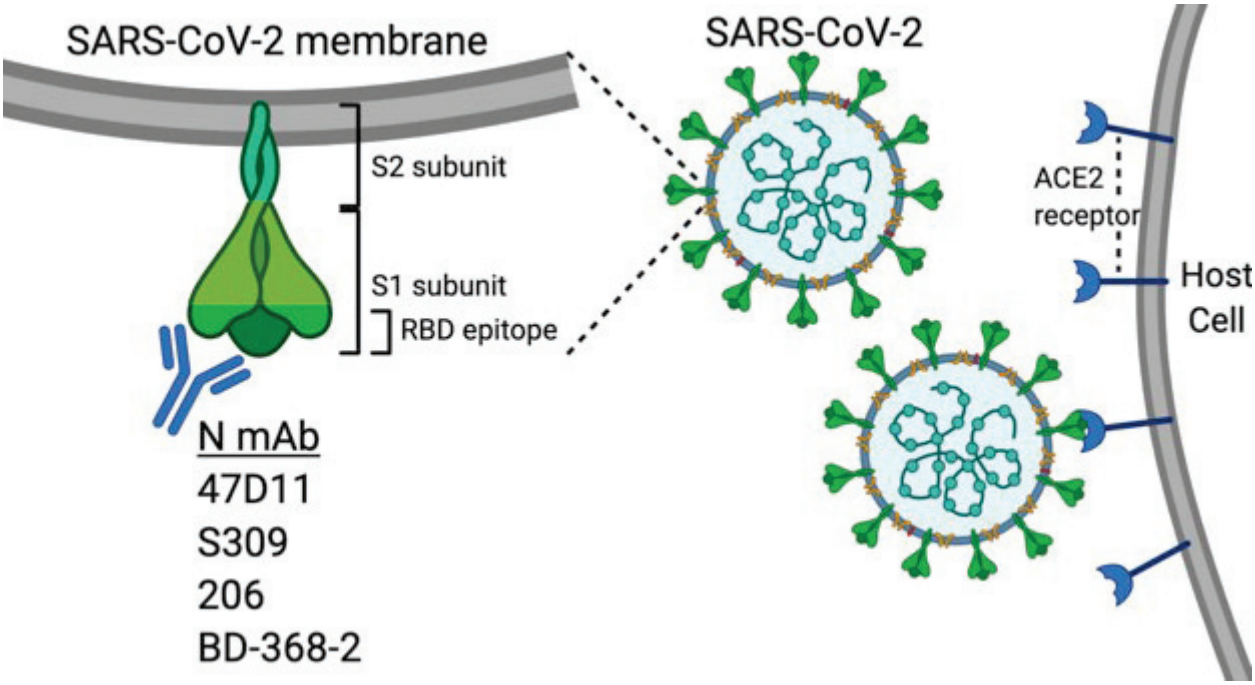

Anti-SARS-CoV-2 neutralizing monoclonal antibodies. SARS-CoV-2 infects host cells through the ACE2 receptor. 47D11, S309, 206, BD-368-2 nAbs bind to RBD site of SARS-CoV-2 Spike and neutralize them.

Chapter 2.

Specific Substitutions in Region V2 of gp120 *env* confer SHIV Neutralisation Resistance

2.1. Abstract

A tier 2 SHIV-MK38 strain was obtained after two in vivo passages of tier 1 SHIV-MK1. SHIV-MK38#818, cloned from the MK38 strain, was neutralisation-resistant, like the parental MK38 strain, to SHIV-infected monkey plasma (MP), HIV-1-infected human pooled plasma (HPP), and KD247 monoclonal antibody (mAb) (anti-V3 gp120 *env*). I investigated the mechanisms underlying the resistance of #818, specifically the amino acid substitutions that confer resistance to MK1. I introduced amino acid substitutions in the MK1 envelope by in vitro mutagenesis and then compared the neutralisation resistance to MP, HPP, and KD247 mAb with #818 in a neutralisation assay using TZM-bl cells. I selected 11 substitutions in the V1, V2, C2, V4, C4, and V5 regions based on the alignment of *env* of MK1 and #818. The neutralisation resistance of the mutant MK1s with 7 of 11 substitutions in the V1, C2, C4, and V5 regions did not change significantly. These substitutions did not alter any negative charges or N-glycans. The substitutions N169D and K187E, which added negative charges, and S190N in the V2 region of gp120 and A389T in V4, which created sites for N-glycan, conferred high neutralisation resistance. The combinations N169D+K187E, N169D+S190N, and N169D+A389T resulted in MK1 neutralisation resistance close to that of #818. The combinations without 169D were neutralisation-sensitive. Therefore, N169D is the most important substitution for neutralisation resistance. This study demonstrated that although the V3 region sequences of #818 and MK1 are the same, V3 binding antibodies cannot neutralise #818 pseudovirus. Instead, mutations in the V2 and V4 regions inhibit the neutralisation of anti-V3 antibodies. I hypothesised that 169D and 190N altered the MK1 Env conformation so that the V3 region is buried. Therefore, the V2 region may block KD247 from binding to the tip of the V3 region.

2.2. Introduction

Simian immunodeficiency virus (SIV) has been used to study the pathogenesis of AIDS, and in vaccine development. However, the Env structures and antigenicity of SIV and HIV differ and have low homology. Therefore, this model is inappropriate for analysing the role of neutralising antibody in protective immunity. To overcome this problem, the HIV-1 *env* gene was inserted into the SIV genome, which lacks its own *env* gene, and simian/human immunodeficiency viruses (SHIVs) were constructed [1,2].

SHIVs were infectious in rhesus macaques (*Macaca mulatta*) and became highly pathogenic after in vivo adaptation [3,4]. Nevertheless, the initial SHIV89.6p macaque model could not predict the effects of candidate vaccines in the human clinical trial (STEP trial) conducted by Merck in 2007. This failure was mainly attributed to differences in coreceptor use and resistance to neutralising antibodies between SHIV89.6p and HIV-1. SHIV89.6p uses CXCR4 (X4) as the main coreceptor and is sensitive to neutralising antibodies (tier 1), whereas circulating HIV-1s use CCR5 (R5) and are antibody-resistant (tier 2) [5].

In 2010, Matsuda et al. constructed R5 tropic SHIV-MK1 via five amino acid substitutions in the *env* V3 region of tier 1 X4 tropic SHIV-KS661, based on the consensus amino acid alignment analyses of subtype B R5 HIV-1; however, MK1 was still tier 1 [6]. Therefore, they passaged MK1 in vivo and obtained a tier 2 MK38 strain as a mixture of viruses after two passages. Then, MK38#818, which is neutralisation-resistant to HIV-1-infected human plasma, similar to the parental SHIV-MK38, was cloned from the MK38 strain [5].

Matsuda et al. compared the gp120 V1, V2, and V3 amino acid alignments of SHIV-KS661 and 14 SHIV-MK38 clones. On checking the positions of the amino acid substitutions in the 14 clones, the majority of the MK38 clones contained substitutions in the V1 region, and some had

substitutions in V2 [6]. Subsequently, Ishida et al. sequenced the complete *env* genes of the MK38 series and identified the substitutions between SHIV-MK1 and MK38#818 (Figure 1c). However, neither Ishida et al. nor Matsuda et al. examined the roles of the substitutions in neutralisation resistance.

Here, I investigated the cause of the resistance of #818, specifically the amino acid substitutions that make MK1 resistant. I introduced amino acid substitutions into the MK1 *env* gene by in vitro mutagenesis based on the amino acid alignment of the MK1 and MK38 virus strains, and then compared their neutralisation resistance.

2.3. Results

2.3.1. Neutralisation of MK1 (tier 1) and #818 (tier 2) in MK1- and #818-Infected MP and HIV-1-Infected Human Pooled Plasma (HPP)

First, I sought to generalise the adaptation of HIV in humans to monkeys, because neither Ishida et al. nor Matsuda et al. examined the neutralisation resistance of SHIV-MK1 and SHIV#818 against SHIV-infected monkey plasma (MP) [5,6]. Therefore, I assessed whether MP represented HPP by comparing the neutralisation resistance of SHIV-MK1 (tier 1B), SHIV-MK38#818 (tier 2), and the control strains HIV-1 TRO (tier 2) and HIV-1 SF162 (tier 1A) with the TZM-bl assay.

I used tier 1 SHIV-infected MP, such as MK1 (MK1 inf. MP), to determine whether plasma induces tier 1 antibodies. While MK1 inf. MP prepared 16 weeks post-infection (wpi) efficiently neutralised MK1 (tier 1B) and SF162 (tier 1A), this plasma did not neutralise either #818 or TRO. This indicates that MK1 inf. MP 16 wpi contained tier 1, but not tier 2, antibodies (Figure 2a).

The MK1 inf. MP at 104 wpi efficiently neutralised MK1 and SF162, and contained a low titre of antibodies that neutralise #818; however, it did not neutralise TRO. Therefore, 104 wpi plasma can strongly induce tier 1A and 1B antibodies, and can trigger the induction of tier 2 antibodies for #818 (Figure 2b). MK1 inf. MP at 104 wpi could not induce tier 2 antibodies for #TRO, but it could induce tier 2 antibodies for #818 because #818 is molecular clone of MK1.

Next, I used tier 2 SHIV-infected MP (i.e., #818 inf. MP) to examine whether the macaque plasma induced tier 2 antibodies. While the antibodies elicited in #818 inf. MP at 12 weeks post #818 infection neutralised MK1 and SF162 efficiently, they did not neutralise either #818 or TRO. This indicates that #818-infected monkey 12 wpi plasma can induce tier 1A and 1B antibodies (Figure 2c). MK1 inf. MP at 16 wpi and #818 inf. MP at 16 wpi are similar.

The #818 inf. MP at 51 weeks post-#818 infection efficiently neutralised MK1(3400×) and SF162 (17,000×), and neutralised #818 to some degree (350×), but it could not neutralise TRO. This indicates that #818 inf. MP at 51 wpi contained tier 1 and 2 antibodies that neutralise #818 (Figure 2d). While #818 inf. MP at 51 wpi could induce tier 2 antibodies for #818, it could not induce tier 2 antibodies for #TRO.

I also determined the ID_{50} of SHIV-MK1 and #818 against HPP, and found that the ID_{50} of HIV-1 reference clone tier 1A SF162 was 1:11,110, while that of tier 2 HIV-TRO was 1:153. The ID_{50} of SHIV-MK1 was 1:550 and that of MK38#818 was 1:138 (Figure 2e). The ID_{50} of #818 against HPP was 3.9-fold greater than that of MK1. The neutralisation resistance patterns of MK1 and #818 against #818-infected MP at 51 wpi, MK1 infected MP at 104 wpi, and HIV-1-infected HPP were similar. These results also demonstrate that monkey experiments for HIV research remain preliminary.

2.3.2. Neutralisation of MK1 and #818 by each Monoclonal Antibody (mAb)

To characterise the neutralisation properties of MK and #818, I examined the effects of several mAbs on known epitopes to determine the dominant mAb representing HIV-1-infected HPP:

- The 50% inhibition concentrations (IC_{50}) of TRO, #818, MK1, and SF162 against VRC01 (gp120 CD4bs) were within 0.3 μg mL^{-1} (Figure 3a).
- The IC_{50} of #818, MK, and SF162 against anti-HIV-1 gp41 mAb 2F5 was <3 μg mL^{-1}, while the IC_{50} of TRO was > 10 μg mL^{-1} (Figure 3b). The neutralisation resistance to 2F5 is similar between MK and #818.

- The IC_{50} values of MK1 and #818 against mAb PG9 (gp120 V2 N-glycan) and mAb PG16 (gp120 V2 N-glycan) are > 10 μg mL^{-1} and are similar to each other (Figure 3c,d).
- The IC_{50} values of MK1, #818, SF162, and TRO against mAb PGT121 and PGT 126 (gp120 V3 N-glycan) were <0.1 μg mL and were similar to each other (Figure 3e, f).
- The IC_{50} values of MK1, #818, SF162, and TRO against mAb 2G12 (gp120 C2V3C3V4C4 N-glycan) were 10, 5, 3.4, and 0.6 μg/μL, respectively (Figure 3g). The IC_{50} values of MK and #818 against 2G12 were not like those against HPP.
- While the IC_{50} of #818 against KD247 mAb (IGPGR epitope on gp120 V3) is >50 μg mL^{-1}, that of TRO is around 50 μg mL^{-1}, the IC_{50} values of MK1 and SF162 are 0.55 and 0.047 μg mL^{-1}, respectively. #818 had more than 100 times greater neutralisation resistance to KD247 than did MK1 (Figure 3h).

I found that the neutralisation analysis patterns of MK1 inf MP at 104 wpi, #818 inf. MP at 51 wpi, HIV-1 inf HPP, and KD247 were similar, while most of the Abs in MK1 inf MP at 104 wpi, #818 inf. MP at 51 wpi, and HIV-1 inf HPP were similar to KD247 mAb (Figure 2; Figure 3h). The other antibodies did not yield similar results (Figure 3). I selected the antibody closest to KD247 mAb as representative of HIV-1-infected HPP and SHIV-infected MP.

2.3.3. Neutralisation of Consensus Pseudoviruses in KD247

I analysed the sequence variation of the MK38 strain and identified four majority consensus mutations in the 13 substitutions in the #818 clone: K187E, S190N, A389T, and T437A. Then, *env* consensus mutants for MK1 were generated using a mutagenesis method: MK1+K187E (E), MK1+K187E+S190N (EN), MK1+K187E+S190N+A389T (ENT), and

MK1+K187E+S190N+A389T+ T437A (ENTA). I performed neutralisation assays using KD247 mAb.

The IC_{50} values of MK-1 and its consensus clones against KD247 were <10 μg $μL^{-1}$; the IC_{50} values of #818 were >50 μg $μL^{-1}$. Like MK1, the consensus MK1s mutant clones were sensitive to KD247 mAb (Figure 4).

2.3.4. Neutralisation of MK1 Mutant Molecular Clones with 169D in KD247

None of the consensus MK1 mutant clones showed resistance similar to that of #818 against KD247. ENTA, with the four consensus MK1 mutants, had better neutralisation resistance to KD247 than did MK1 (Figure 4). The consensus MK1+ENTA has 187E, which results in a negative charge, and 190N in the V2 region of gp120 and 389T in V4, which create sites for N-glycan.

However, Matsuda et al. reported that the amino acid substitutions in the V2 region in the 14 MK38 clones were N169D, K187E, and S190N [6]. I also examined the mutations in #818 env. N169D in the V1V2 region also caused an added negative charge, like K187E. Therefore, I added N169D to the consensus MK1+ENTA using a mutagenesis method.

Notably, the IC_{50} of the consensus MK1+ENTA with N169D was >50 μg mL^{-1}, similar to that of #818 against KD247. The IC_{50} of the consensus MK1+ENTA was <10 μg mL^{-1} (Figure 5a). The addition of 169D to MK1+ENTA increased the neutralisation resistance markedly (Figure 5a). I also added N169D to the other consensus MK1s (i.e., MK1+E, MK1+EN, MK1+ENT, and MK1+ENTA), including in various different combinations to obtain resistant MK1 with minimal mutations, including 169D. Therefore, I generated DENT (MK1env+N169D+K187E+S190N+A389T), DEN, DNT, DE, DN, DT, and D to determine

which mutations are important for neutralisation resistance against KD247 when combined with N169D. I also tested neutralisation resistance against KD247 with other substitutions, i.e., N133S, S147G, N169D, N237T, D282N, S294F, T437A, and T463P with MK1, but did not see any difference from the consensus MK1s (<10 μg mL^{-1}; data not shown).

The IC_{50} values of #818, DENTA, DENT, DEN, DNT, DE, DN, and DT against KD247 were similar, and were all >50 μg mL^{-1} (Figure 5b, c). While the IC_{50} of MK1 was 0.5 μg mL^{-1}, that of MK1+ N169D was 17 μg mL^{-1}. The IC_{50} of MK1+169D indicated more than 34 times greater neutralisation resistance to KD247 compared to MK1 (Figure 5c).

The DEN, DE, DN, and DT viruses had MK1 neutralisation resistance close to that of #818, which was similar to tier-2 TRO. Moreover, the DENTA, DENT, and DNT viruses were as MK1 neutralisation-resistant as #818 (Figure 5a–c). In summary, the consensus mutant MK1s with 169D were neutralisation-resistant against KD247. Therefore, N169D is a key substitution for acquiring neutralisation resistance.

2.3.5. Neutralisation of MK1 Mutant Molecular Clones with 169D in HPP

I already showed that most of the Abs in HIV-1-infected HPP are like KD247 mAb. The IC_{50} values of #818, DENTA, DENT, DEN, DNT, DE, DN, and DT against KD247 were > 50 μg mL^{-1}. Accordingly, consensus mutant MK1s with 169D might be tier 2 viruses, such as #818 and TRO. To confirm this, I also determined the ID_{50} of consensus mutant MK1s with 169D against HPP.

The ID_{50} values of DENT, DEN, #818, DNT, and TRO were 1:240 against HPP, while the ID_{50} of MK1 was 1:960, and those of DN and DE were 1:320 and 1:350, respectively (Figure 6).

I discovered that DENTA, DENT, DEN, and DNT had tier 2 resistance, like #818 and TRO. I created new tier 2-resistant viruses by adding to the negative charge of 169D in MK1 with a minimum of two consensus mutations.

2.3.6. Neutralisation of MK1 Mutant Molecular Clones with 169D in SHIV-infected MP

After determining that SHIV-infected late wpi MP mimicked HIV-1-infected HPP, I also evaluated whether this was effective for molecular clones with 169D.

I determined the ID_{50} values of DENT, DEN, and DNT, and compared MK1 and 818. The ID_{50} values of DENT, DNT, DEN, 818, and MK1 against MK1-infected MP at 104 wpi were 1:150, 1:130, 1:250, 1:380, and 1:9500, respectively (Figure 7a). The neutralisation resistances of all consensus MK1s with 169D were slightly higher than that for 818 against MK1 inf MP at 104 wpi.

I also determined the ID_{50} values of DENT, DNT, DEN, 818, and MK1 against #818 inf. The MP at 51 wpi for MP was 1:140, 1:160, 1:160, 1:350, and 1:2600, respectively (Figure 7b). The neutralisation resistance of all consensus MK1s with 169D was also slightly higher than that for 818 against #818 inf. MP 51 wpi (Figure 7a, b). Thus, DENT, DNT, and DEN have tier 2 resistance, like #818 and TRO.

2.4. Discussion

I investigated the cause of the resistance of #818 in detail, specifically the amino acid substitutions that make MK1 resistant. The V1V2 region of HIV strains shows great variety because it contains many substitutions, deletions, and insertions. This variety enables escape from the immune response and high resistance to specific neutralising antibodies. The other features of V1V2 are that it is somewhat longer, and has more glycosylated sites, than historical viruses [14].

The neutralisation resistance of MK1+DENT, MK1+DEN, and MK1+DNT with the V1V2 and V4 substitutions was similar to that of #818 and TRO against KD247. The negative charges at 169D and 187E, and the N-glycan 190N and 389T substitutions, are important for the neutralisation resistance. I discuss each of these substitutions in the following sections.

2.4.1. Position 169 (167 in HXB2)

While amino acid substitutions in the V1 region had no effect on neutralisation resistance, the amino acid substitutions in the V2 region did affect the neutralisation resistance. The main reason for this is that the amino acid substitutions in the V1 region obtained in our experiments did not lead to any charge changes or N-linked glycosylation sites. In comparison, the substitutions in the V2 region resulted in changes in two electrical charges (N169D and K187E) and one N-linked glycosylation site (S190N) (Figure 1). The V1/V2 fold, also known as the 'Greek key', contains four anti-parallel protein strands (A–D) between strands β2 and β3 of the core gp120 [15]. Arginine (R) and lysine (K) frequently form salt bridges by pairing with negatively charged aspartate (D) or glutamate (E), to create hydrogen bonds that stabilize the protein structure (salt bridges are generally K-D or D-R) [16]. I hypothesised that 169D (167 in HXB2) is important for maintaining the C strand of the Greek key because it is located at the tip of the C strand and could be involved in hydrogen bonding/salt bridges. In addition, 169D is

included in peptides 167–178 of the C strands (IRDKVKKEYALF) of both TRO and #818. The formation of these hydrogen bonds/salt bridges could alter the three-dimensional conformation of the V1/V2 region. Therefore, N169D is a key substitution for acquiring neutralisation resistance.

2.4.2. Position 187 (184 HXB2)

The neutralisation resistances of #818, MK1+DENT, MK1+DEN, and MK1+DNT against KD247 were similar, and were all >50 µg/mL (Figure 5b). As shown in the figure, 187E seemed to have no effect on the neutralisation resistance. To verify this, I also performed a neutralisation resistance assay against KD247 with a minimum of two amino acid changes, including 169D (Figure 5c). The neutralisation resistances of DE, DN, DT, TRO, and #818 were all > 50 µg/mL. The neutralisation resistance of DE was closer to that of #818 compared to DN and DT. Therefore, 187E also had a positive effect on the neutralisation resistance. Like 169D, 187E can also create salt bridges/hydrogen bonds with R or K in peptides 167–178 (IRDKVKKEYALF), thus increasing the stability of the V1/V2 region.

2.4.3. Position 190 (187 HXB2)

The 190N-gylcan (187 in HXB2) in #818 increased the neutralisation resistance in combination with 169D. This is consistent with Li et al. [17], who showed that the removal of a single N-glycan at amino acid position 187 increases the sensitivity of HIV 89.6 to broadly neutralising anti-CD4bs mAb b12 and anti-V3 mAb 447-52D in vitro. Wang et al. [18] also reported that the removal of specific N-glycosylation sites has a significant effect on viral infectivity and neutralisation resistance.

2.4.4. Position 389 (388 HXB2) NXT

The addition of a glycan at position 387 (386 HXB2), with the substitution of T at 389 in #818, increased the neutralisation resistance in combination with 169D. The asparagine (N) at position 386 in HXB2 gp120, which corresponds to the N at position 387 in MK1, is not essential for protein folding or function, but is involved in immune evasion [19]. Furthermore, the loss of an N glycan at position 386 triggers a change in the structure of the V4 loops, leading to a change in the conformation of the CD4 binding site. These changes increased the sensitivity of MVC-resistant virus to sCD4 and b12 [20]. Our results showed that 386T affects V3 antigenicity by covering the V3 site with the mutated V4 region. Therefore, the structural change in V4 may greatly affect the antigenicity of gp120. This is consistent with Li et al., who indicated that the gp120 V4–V5 regions play an important role in fusion efficiency, while the V4 mutations at positions 407D and 386N regulate the resistance to CCR5 antagonists [7,21].

The neutralisation assay results against HPP and MP confirm that MK1 is a tier 1 virus and #818 is a tier 2 virus. When I characterised the neutralisation properties of MK and #818 using mAbs such as VRC01 for CD4bs, 2F5 for gp41, 2G12 for the N-glycan sites of gp120, PG9 for V1V2, and PGT121, PGT126, and KD247 for V3 sites (Figure 3), only the KD247 mAbs produced a similar pattern between HPP and MP (Figure 3). Most of the antibodies in HPP and MP are like KD247, and bind to the V3 region of gp120 *env* (Figures 1–3).

The mutations acquired by #818 were not located in the epitopes of the VRC01, 2F5, PGT121, or KD247 mAbs. KD247 binds the PGR epitope in the V3 region, and efficiently neutralises CXCR4- and CCR5-tropic HIV-1 in primary clade B [22]. However, while KD247 neutralised MK1 and SF162 efficiently, it did not neutralise #818 or TRO (Figure 3h). Note that the V3 site

amino acid sequences of #818 and MK1 are the same, and both also have the same epitope as PGR for KD247 at the V3 site (Figure 8a-c-e).

I postulated that this problem arose because of the trimer conformation, where the neutralisation tier could be determined based on the spike in trimeric HIV-1 envelope glycoprotein. The trimer conformations of tier 2–3 HIV-1 viruses resistant to neutralising antibodies are closed and stabilised, while that of the more sensitive tier 1A strains is open, and that of the somewhat sensitive tier 1B viruses is intermediate [25,26]. Accordingly, MK1 and KS661 might have intermediate trimer structures (Figure 8a-c-e) because, as tier 1B viruses [2], they were neutralised by KD247 mAb. SF162 might also have an open trimer structure because it is a tier 1A virus. However, the KD247 mAb neutralised SF162 more than MK1 and KS661 (Figure 3h). The KD247 mAb can neutralise open and intermediate trimer structures, such as SF162, MK1, and KS661.

TRO and #818 may have closed trimer structures (Figure 8b-d-f) because they are tier 2 viruses. Neither #818 nor TRO was neutralised by the KD247 mAb. The PGR epitope of KD247 is at the apex of the V3 area, and this epitope might be under the V1V2 site (shown in yellow in Figure 8b-d-f). In 2016, Ishida et al. also reported that the neutralisation resistances against KD247 of the tier 2 viruses HIV-PVO.4 and SHIV-MK38 were >50 μg/μL. Accordingly, there is a relationship between the trimer conformation and neutralisation resistance against KD247. Although the tier 2 QH0692.42, PVO.4, AC10.0.29, REJO4541.67, RHPA4259.7, CAAN5342.A2, WITO, RHPA, TRJO, and SUMA viruses have the PGR epitope, their neutralisation resistances against KD247 were all >150 μg/μL [27].

I found that the most important amino acid substitutions and epitopes of the mAbs of MK1 and #818 fit the tier 1 (Figure 8a-c-e) and tier 2 (Figure 8b-d-f) virus models visualised with UCSF Chimera software.

Subsequently, I aimed to find amino acid substitutions that change the conformation and neutralisation resistance. Interactions between the V1V2 domains of different gp120 subunits help stabilise the trimer apex and, consequently, the entire trimer; additional interactions with the V3 domain stabilise the pre-fusion conformation of the trimer, in which the V3 domain is sequestered underneath the V1V2 loops [28]. This reduces the local V2 flexibility and improves the binding of V2-dependent bNAbs and gl-bNAbs [28]. Furthermore, overcoming *env* metastability is central to trimer-based HIV-1 vaccine design [29].

In summary, I speculate that negative charges, such as N169D (aspartic acid) and K187E, can alter the MK1 Env conformation so that the V3 region is buried. In addition, S190N+A389T can also increase the stability. As a result of substitutions N169D + K187E + S190N at V2 sites and A389T at a V4 site, the PGR epitope of KD247 at the apex of the V3 area might be under the V1V2 site (Figure 8b-d-f). A sensitive three-dimensional trimer modelling system may be needed to demonstrate our hypothesis.

2.5. Materials and Methods

2.5.1. Cell Lines

The 293T cells [30] were maintained in Dulbecco's modified Eagle's medium (DMEM) (Wako Pure Chemicals) supplemented with 10% fetal bovine serum (FBS) and 1 mM L-glutamine. TZM-bl cells [31] from the National Institutes of Health (NIH) AIDS Research and Reference Reagent Program were maintained in DMEM with 10% FBS, 1 mM L-glutamine, and 1 mM sodium pyruvate. Cells were harvested and passaged using trypsin/ethylenediaminetetraacetic acid solution (Nacalai Tesque, Kyoto, Japan) and were maintained at 37 °C in a humidified atmosphere containing 5% CO_2.

2.5.2. Generation of the New Vector Plasmid "ZaferY" (pcDNA 3.1/Hygro(+) ΔKpnIΔXhoI)

To examine the size of SHIV env on agarose gel electrophoresis, manipulated pcDNA3.1/Hygro(+), because SHIV env and the vector both contain *Kpn*I and *Xho*I sites. To eliminate the *Kpn*I site, it was digested with *Hin*dIII HF at 37°C for 15 min. The vector was ligated with ligation mix at 16 °C for 30 min. To delete the *Xho*I site in the vector, it was digested with *Not*I and *Apa*I, blunt-ended using T4 DNA polymerase, and self-ligated. This new vector was called "ZaferY".

2.5.3. Generation of Pseudoviruses

The pSHIV-KS661 *env* gene, pSHIV-MK1 *env* gene, and pSHIV-#818 with the pUC119 vector *env* gene were obtained from the Research Centre for Infectious Diseases Primate Laboratory of the Institute for Frontier Life and Medical Science (Kyoto University, Kyoto, Japan). A 2-kb DNA fragment containing *env* was subcloned into ZaferY vector following digestion with the restriction enzymes *Kpn*I and *Xho*I.

2.5.4. Construction of Mutant MK1 env Clones

Mutant MK1 strains were generated using the KOD-Plus-Mutagenesis Kit (Toyobo, Osaka, Japan). These included N133S, S147G (V1 region), N169D, K187E, S190N (V2 region), N237T, D282N, S294F (C2 region), A389T (V4 region), T437A (C4 region), and T463P (V5 region).

PCR consisted of an initial denaturation (94 °C for 2 min), nine amplification cycles (98 °C for 30 s, 53 °C for 30 s, and 68 °C for 8 min 24 s), and a final extension (68 °C for 8 min 24 s). The reactions consisted of 35 µL of PCR-grade water, 5 µL of KOD Plus 10× buffer, 5 µL of 2 mM dNTPs, 1.5 µL of 10 pmol/µL primers F and R, 1 µL of KOD Plus DNA Polymerase (Toyobo) and 1 µL of 50 ng/µL as template. The following primers were used for the mutagenesis assays.

A6843G (N169D)	F primer (5′-GATAAGGTAAAGGAAAGAATATGCAC-3′)
	R primer (5′-TCTTATGCTTGTGGTGATATAGAAA-3′)
A6897G (K187E)	F primer (5′-GAAAATACTAGTAATACTAAGTATAGGT-3′)
	R primer (5′-TACTGGTACTACATCAAGTCTATTAAAA-3′)
G6907A (S190N)	F primer (5′-ATAATACTAAGTATAGGTTAATAAGTTG-3′)
	R primer (5′-TAGTATTTTTTACTGGTACTACATC-3′)
G7503A (A389T)	F primer (5′-ACACAACTGTTTAATAGTACTTGGAATG-3′)
	R primer (5′-TGTATTACAGTAGAAAAATTCCCCTCCA-3′)
A6736G (N133S)	F primer (5′-GTTTGAATATCACTAAGAATACTACTAATC-3′)
	R primer (5′-TAGTGCAATTTAAAGTAACACAGAGTGGG-3′)
A6777G (S147G)	F primer (5′-GGCTGGGGAATGATGGAGGAAGGAGAAATA-3′)
	R primer (5′-GCTACTAGTGAGATTAGTAGTATTCTTAGT-3′)
A7048C (N237T)	F primer (5′-CTGGATCAGGACCATGCACAAAT-3′)
	R primer (5′-TGAATGTCTTATTGTTACACTTTAGTATCG-3′)
G7182A (D282N)	F primer (5′-AACAATGTTAAAACCATAATAGTACAGCTA-3′)
	R primer (5′-TGTGAAATCTTCAGATCTAATTACTATGTC-3′)
C7219T (S294F)	F primer (5′-TTGTAGTAATTAATTGTACAAGACC-3′)
	R primer (5′-ATTCATTTAGCTGTACTATTATGGT-3′)
A7647G (T437A)	F primer (5′-GCAGGACAAATTAGATGTTCATCAAATA-3′)
	R primer (5′-GATGGGAGGGGCATACATTGCTTTTCCT-3′)

2.5.5. Isolation of MP from Infected Rhesus Macaques

In 2010, Matsuda et al. constructed R5 tropic SHIV-MK1 by introducing five amino acid substitutions in the *env* V3 area of tier 1 HIV-1 X4 tropic SHIV-KS661 based on a consensus amino acid alignment analysis of subtype B R5 HIV-1; nevertheless, MK1 was still tier 1 [6]. Therefore, they passaged MK1 intravenously in a rhesus macaque (MM482). To allow MK1 to adapt, it was passaged in vivo from macaque MM482 to one uninfected macaque (MM498) and then to a second uninfected macaque (MM504).

After these two passages, they obtained a tier 2 MK38 strain as a mixture of viruses. Three uninfected rhesus macaques (MM481, MM501, and MM502) were infected with MK38 intravenously [6]. Then, MK38#818, which was neutralisation-resistant to HIV-1-infected human plasma, like the parental SHIV-MK38, was cloned from the MK38 strain [5]. The uninfected rhesus macaque MM597 was infected by tier 2 #818 to study the pathogenesis of HIV [5]. MP was collected from the infected macaques MM481 (MK1 infected macaque) and MM597 (#818 infected macaque) and stored at −80 °C.

The Indian rhesus macaque experiments were performed in a biosafety level 3 facility in the Institute for Frontier Life and Medical Sciences Primate Laboratory, in accordance with the institutional regulations of the Committee for the Experimental Use of Non-human Primates.

2.5.6. Neutralisation Assays

To evaluate virus neutralisation resistance, I performed neutralisation assays using plasma at 16 and 104 wpi from the SHIV-MK1-infected MM482 monkey, plasma at 12 and 51 wpi from the SHIV-MK38#818-infected MM597 monkey, pooled plasma from HIV-1-infected individuals (ZeptoMetrix, Buffalo, NY, USA), and anti-HIV-1 monoclonal neutralisation antibodies. In the assays, luciferase activity was measured using TZM-bl cells [32]. The details of the neutralisation assays have been described elsewhere [5,6].

The pooled plasma of HIV-1-infected individuals was diluted three-fold, from 1:60 to 1:1180980. MK38#818- and MK1-infected MP were diluted two-fold from 1:60-1:30720. Subsequently, the ID_{50} was calculated as described earlier [25].

Six anti-HIV-1 monoclonal neutralising antibodies were used. KD247, which recognises the GPGR epitope in the V3 region of gp120, was kindly provided by the Centre for AIDS Research (Kumamoto University, Kumamoto, Japan). PGT121, 2F5, VRC01, 2G12, and PG9 were provided by Dr. Bruce Brown through the NIH AIDS Reagent Program (Germantown, MD, USA). KD247 was diluted three-fold from 50 to 0.001 µg/mL; 2F5, VRC01, 2G12, and PG9 were diluted two-fold from 10 to 0.015 µg/mL; and PGT121 was diluted two-fold from 0.1 to 0.002 µg/mL. The IC_{50} values were then calculated as described earlier [25].

2.6. Conclusions

I introduced amino acid substitutions into the envelope of MK1 by in vitro mutagenesis and then compared the neutralisation resistance to MP, HPP, and KD247 mAb with #818 in neutralisation assays using TZM-bl cells. Based on the alignment of *env* of MK1 and #818, I selected 11 substitutions: N133S, S147G (V1 region), N169D, K187E, S190N (V2 region), N237T, D282N, S294F (C2 region), A389T (V4 region), T437A (C4 region), and T463P (V5 region). The neutralisation resistance of the mutant MK1s that harboured 7 of the 11 substitutions (N133S, S147G, N237T, D282N, S294F, T437A, and T463P) did not change significantly. These substitutions did not affect any negative charges or N-glycans. However, higher neutralisation resistance was conferred by the N169D and K187E substitutions, which added negative charges, and the S190N (V2 region of gp120) and A389T (V4 region) substitutions, which created sites for N-glycan. The combinations N169D+K187E, N169D+S190N, and N169D+A389T led to MK1 having similar neutralisation resistance to #818, while the combination N169D +S190N+ A389T led to identical neutralisation resistance between MK1 and #818. The combinations without 169D were neutralisation-sensitive. Therefore, N169D of V2 region is a key substitution for acquiring neutralisation resistance against anti-V3 antibodies. These findings illuminate a genetic aspect of how HIV may evade deactivation by the B cell mediated adaptive immunity.

2.7. References

1. Shibata, R.; Kawamura, M.; Sakai, H.; Hayami, M.; Ishimoto, A.; Adachi, A. Generation of a chimeric human and simian immunodeficiency virus infectious to monkey peripheral blood mononuclear cells. *J. Virol.* 1991, *65*, 3514–3520.
2. Ishida, Y.; Miura, T. Nonhuman primate models for empirical research of acquired immunodeficiency syndrome. *Ann. Virol. Res.* 2016, *2*, 1016.
3. Shinohara, K.; Sakai, K.; Ando, S.; Ami, Y.; Yoshino, N.; Takahashi, E.; Someya, K.; Suzaki, Y.; Nakasone, T.; Sasaki, Y.; et al. A highly pathogenic simian/human immunodeficiency virus with genetic changes in cynomolgus monkey. *J. Gen. Virol.* 1999, *80*, 1231–1240, doi:10.1099/0022-1317-80-5-1231.
4. Reimann, K.A.; Li, J.T.; Veazey, R.; Halloran, M.; Park, I.-W.; Karlsson, G.B.; Sodroski, J.; Letvin, N.L. A chimeric simian/human immunodeficiency virus expressing a primary patient human immunodeficiency virus type 1 isolate env causes an AIDS like disease after in vivo passage in rhesus monkeys. *J. Virol.* 1996, *70*, 6922–6928.
5. Ishida, Y.; Kato, F.; Hishiki, T.; Matsuura, K.; Miura, T.; Watanabe, Y.; Yoneda, M.; Igarashi, T.; Matsushita, S.; Kikukawa, M.; et al. Generation of a neutralization-resistant CCR5 tropic simian/human immunodeficiency virus (SHIV-MK38) molecular clone, a derivative of SHIV-89.6. *J. Gen. Virol.* 2016, *97*, 1249–1260, doi:10.1099/jgv.0.000421.
6. Matsuda, K.; Inaba, K.; Fukazawa, Y.; Matsuyama, M.; Ibuki, K.; Horiike, M.; Saito, N.; Hayami, M.; Igarashi, T.; Miura, T. In vivo analysis of a new R5 tropic SHIV generated from the highly pathogenic SHIV-KS661, a derivative of SHIV-89.6. *Virology* 2010, *399*, 134–143, doi:10.1016/j.virol.2010.01.008.

7. Wu, X., Yang, Z. Y., Li, Y., Hogerkorp, C. M., Schief, W. R., Seaman, M. S., . . . Mascola, J. R. (2010). Rational design of envelope identifies broadly neutralizing human monoclonal antibodies to HIV-1. Science, 329(5993), 856-861. doi:10.1126/science.1187659

8. Purtscher, M., Trkola, A., Grassauer, A., Schulz, P. M., Klima, A., Dopper, S., . . . Katinger, H. (1996). Restricted antigenic variability of the epitope recognized by the neutralizing gp41 antibody 2F5. AIDS, 10(6), 587-593.

9. Walker, L. M., Phogat, S. K., Chan-Hui, P. Y., Wagner, D., Phung, P., Goss, J. L., . . . Burton, D. R. (2009). Broad and potent neutralizing antibodies from an African donor reveal a new HIV-1 vaccine target. Science, 326(5950), 285-289. doi:10.1126/science.1178746

10. Walker, L. M., Huber, M., Doores, K. J., Falkowska, E., Pejchal, R., Julien, J. P., . . . Poignard, P. (2011). Broad neutralization coverage of HIV by multiple highly potent antibodies. Nature, 477(7365), 466-470. doi:10.1038/nature10373

11. Trkola, A., Purtscher, M., Muster, T., Ballaun, C., Buchacher, A., Sullivan, N., . . . Katinger, H. (1996). Human monoclonal antibody 2G12 defines a distinctive neutralization epitope on the gp120 glycoprotein of human immunodeficiency virus type 1. J Virol, 70(2), 1100-1108.

12. Murin, C.D., Julien, J.P., Sok, D., Stanfield, R.L., Khayat, R., Cupo, A., Moore, J.P., Burton, D.R., Wilson, I.A., and Ward, A.B. (2014). Structure of 2G12 Fab2 in complex with soluble and fully glycosylated HIV-1 Env by negative-stain single-particle electron microscopy. J. Virol. 88, 10177–10188.

13. Eda, Y., Takizawa, M., Murakami, T., Maeda, H., Kimachi, K., Yonemura, H., Koyanagi, S., Shiosaki, K., Higuchi, H. & other authors (2006). Sequential immunization with V3 peptides

from primary human immunodeficiency virus type 1 produces crossneutralizing antibodies against primary isolates with a matching narrow-neutralization sequence motif. J Virol 80, 5552–5562.

14. Li, Y.; Dittmer, D.; Wang, W.; Song, J.; Sun, B.; Yang, R. The V1 region of gp120 is preferentially selected during SIV/HIV transmission and is indispensable for envelope function and virus infection. *Virol. Sin.* 2016, *31*, 207–218 doi:10.1007/s12250-016-3725-5.
15. McLellan, J.S.; Pancera, M.; Carrico, C.; Gorman, J.; Julien, J.-P.; Khayat, R.; Louder, R.; Pejchal, R.; Sastry, M.; Dai, K.; et al. Structure of HIV-1 gp120 V1/V2 domain with broadly neutralizing antibody. *Nature* 2011, *480*, 336–343, doi:10.1038/nature10696.
16. Betts, M.J.; Russell, R.B. Amino Acid Properties and Consequences of Substitutions. In *Bioinformatics for Geneticists,* Barnes, M.R., Gray, I.C., Eds.; John Wiley & Sons,Ltd: Hoboken, NJ, USA, 2003.
17. Li, Y.; Cleveland, B.; Klots, I.; Travis, B.; Richardson, B.A.; Anderson, D.; Montefiori, D.; Polacino, P.; Hu, S.L. Removal of a single N-linked glycan in human immunodeficiency virus type 1 gp120 results in an enhanced ability to induce neutralizing antibody responses. *J. Virol.* 2008, *82*, 638–651 0022-538X/08/$08.000 doi:10.1128/JVI.01691-07.
18. Wang, W.; Nie, J.; Prochnow, C.; Truong, C.; Jia, Z.; Wang, S.; Chen, X.S.; Wang, Y. A systematic study of the N-glycosylation sites of HIV-1 envelope protein on infectivity and antibody-mediated neutralization. *Retrovirology* 2013, *10*, 14, doi:10.1186/1742-4690-10-14.
19. Sanders, R.W.; van Anken, E.; Nabatov, A.A.; Liscaljet, I.M.; Bontjer, I.; Eggink, D.; Melchers, M.; Busser, E.; Dankers, M.M.; Groot, F.; et al. The carbohydrate at asparagine 386 on HIV-1 gp120 is not essential for protein folding and function but is involved in immune evasion. *Retrovirology* 2008, *5*, 10, doi:10.1186/1742-4690-5-10.

20. Tilton, J.C.; Wilen, C.B.; Didigu, C.A.; Sinha, R.; Harrison, J.E.; Agrawal-Gamse, C.; Henning, E.A.; Bushman, F.D.; Martin, J.N.; Deeks, S.G.; et al. A Maraviroc-resistant HIV-1 with narrow cross-resistance to other CCR5 antagonists depends on both N-terminal and extracellular loop domains of drug-bound CCR5. *J. Virol.* 2010, *84*, 10863–10876, doi:10.1128/JVI.01109-10.

21. Li, Y.; Yang, D.; Wang, J.Y.; Yao, Y.; Zhang, W.Z.; Wang, L.J.; Cheng, D.C.; Yang, F.K.; Zhang, F.M.; Zhuang, M.; et al. 2014. Critical amino acids within the human immunodeficiency virus type 1 envelope glycoprotein V4 N- and C-terminals contribute to virus entry. *PLoS ONE* 2014, *9*, e86083, doi:10.1371/journal.pone.0086083.

22. Eda, Y.; Murakami, T.; Ami, Y.; Nakasone, T.; Takizawa, M.; Someya, K.; Kaizu, M.; Izumi, Y.; Yoshino, N.; Matsushita, S.; et al. Anti-V3 humanized antibody KD247 effectively suppresses ex vivo generation of human immunodeficiency virus type 1 and affords sterile protection of monkeys against a heterologous simian/human immunodeficiency virus infection. *J. Virol.* 2006, *80*, 5563–5570, doi:10.1128/JVI.02095-05.

23. Rasheed, M.; Bettadapura, R.; Bajaj, C. Computational refinement and validation protocol for proteins with large variable regions applied to model HIV Env spike in CD4 and 17b bound state. *Structure* 2015, *23*, 1138–1149.

24. Peña, A.T.; Rantalainen, K.; Cottrell, C.A.; Allen, J.D.; Gils, M.J.; Torres, J.L.; Crispin, M.; Sanders, R.W.; Ward, A.B. Similarities and differences between native HIV-1 envelope glycoprotein trimers and stabilized soluble trimer mimetics. *PLoS Pathog.* 2019, *15*, e1007920, doi:10.1371/journal.ppat.1007920.

25. Seaman, M.S.; Janes, H.; Hawkins, N.; Grandpre, L.E.; Devoy, C.; Giri, A.; Coffey, R.T.; Harris, L.; Wood, B.; Daniels, M.G.; et al. Tiered categorization of a diverse panel of HIV-1

Env pseudoviruses for assessment of neutralizing antibodies. *J. Virol.* 2010, *84*, 1439–1452, doi:10.1128/jvi.02108 -09.

26. Montefiori, D.C.; Roederer, M.; Morris, L.; Seaman, M.S. Neutralization tiers of HIV-1. *Curr. Opin. HIV AIDS* 2018, *13*, 128–136, doi:10.1097/COH.0000000000000442.
27. Valdez, K.P.R.; Kuwata, T.; Maruta, Y.; Tanaka, K.; Alam, M.; Yoshimura, K.; Matsushita, S. Complementary and synergistic activities of anti-V3, CD4bs and CD4i antibodies derived from a single individual can cover a wide range of HIV-1 strains. *Virology* 2015, *475*, 187–203.
28. De Taeye, S.W.; Go, E.P.; Sliepen, K.; de la Peña, A.T.; Badal, K.; Medina-Ramírez, M.; Lee, W.H.; Desaire, H.; Wilson, I.A.; Moore, J.P.; et al. Stabilization of the V2 loop improves the presentation of V2 loop associated broadly neutralizing antibody epitopes on HIV-1 envelope trimers. *J. Biol. Chem.* 2019, *294*, 5616–5631, doi:10.1074/jbc.RA118.005396.
29. He, L.; Kumar, S.; Allen, J.D.; Huang, D.; Lin, X.; Mann, C.J.; Saye-Francisco, K.L.; Copps, J.; Sarkar, A.; Blizard, G.S.; et al. HIV-1 vaccine design through minimizing envelope metastability. *Sci. Adv*. 2018, *4*, eaau6769, doi:10.1126/sciadv.aau6769.
30. DuBridge, R.B.; Tang, P.; Hsia, H.C.; Leong, P.M.; Miller, J.H.; Calos, M.P. Analysis of mutation in human cells by using an Epstein-Barr virus shuttle system. *Mol. Cell. Biol.* 1987, *7*, 379–387.
31. Platt, E.J.; Wehrly, K.; Kuhmann, S.E.; Chesebro, B.; Kabat, D. Effects of CCR5 and CD4 cell surface concentrations on infections by macrophagetropic isolates of human immunodeficiency virus type 1. *J. Virol.* 1998, *72*, 2855–2864.
32. Wei, X.; Decker, J.M.; Liu, H.; Zhang, Z.; Arani, R.B.; Kilby, J.M.; Saag, M.S.; Wu, X.; Shaw, G.M.; Kappes, J.C. Emergence of resistant human immunodeficiency virus type 1 in

patients receiving fusion inhibitor (T-20) monotherapy. *Antimicrob. Agents Chemother.* 2002, *46*, 1896–1905.

2.8. Figures

Figure 1.

a) Genomic organization of SHIV-MK38 molecular clones.

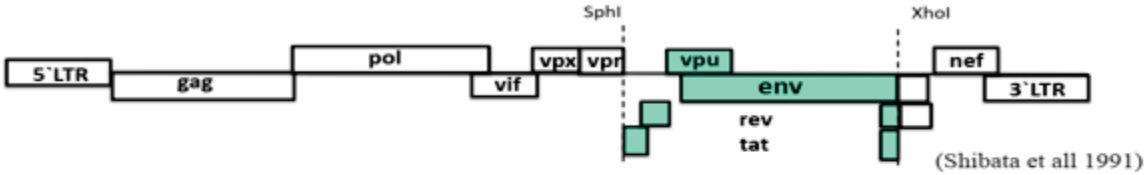

(Shibata et all 1991)

b) Evolution of the SHIV strains.

Name	KS661	MK1	MK38	MK38#818
Coreceptor	X4 (R5)	R5		
Tier	1B		2	
Memo	Molecular clone SHIV89.6 env	The 5 amino acid substitutions in env V3 of KS661	Mutation of MK1	Molecular clone of MK38 env
Figure		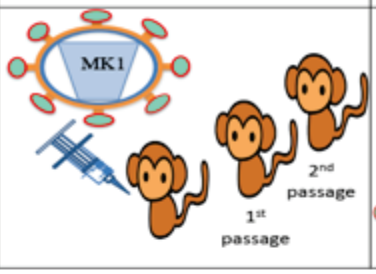	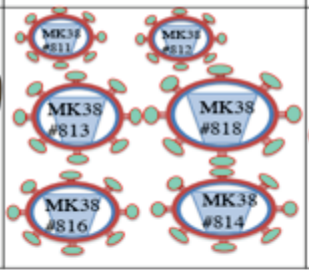	

(Ishida et all, 2016).

c) The amino acid alignment of SHIV-MK1 and SHIV#818.

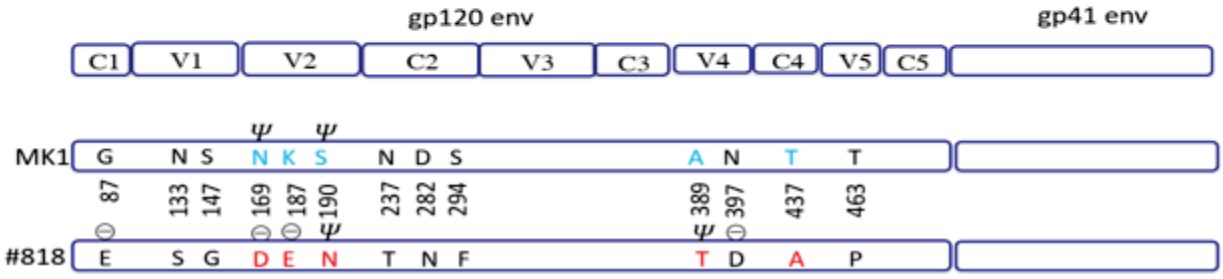

Summary of the SHIV research. (**a**) Genomic organisation of SHIV-MK38 molecular clones generated by replacing the *Sph*I/*Xho*I fragment of SHIV-MK38 (turquoise blue) with the SHIV-KS661 backbone (in white box). (**b**) Evolution of the SHIV strains. (**c**) Amino acid alignment of MK1 env and #818 env. G, glycine; N, asparagine; S, serine; K, lysine; D, aspartic acid; A, alanine; T, threonine; E, glutamic acid; F, phenylalanine; P, proline; ⊖, negative charge; Ψ, N glycan. Blue and red letters indicate the substitutions.

Figure 2.

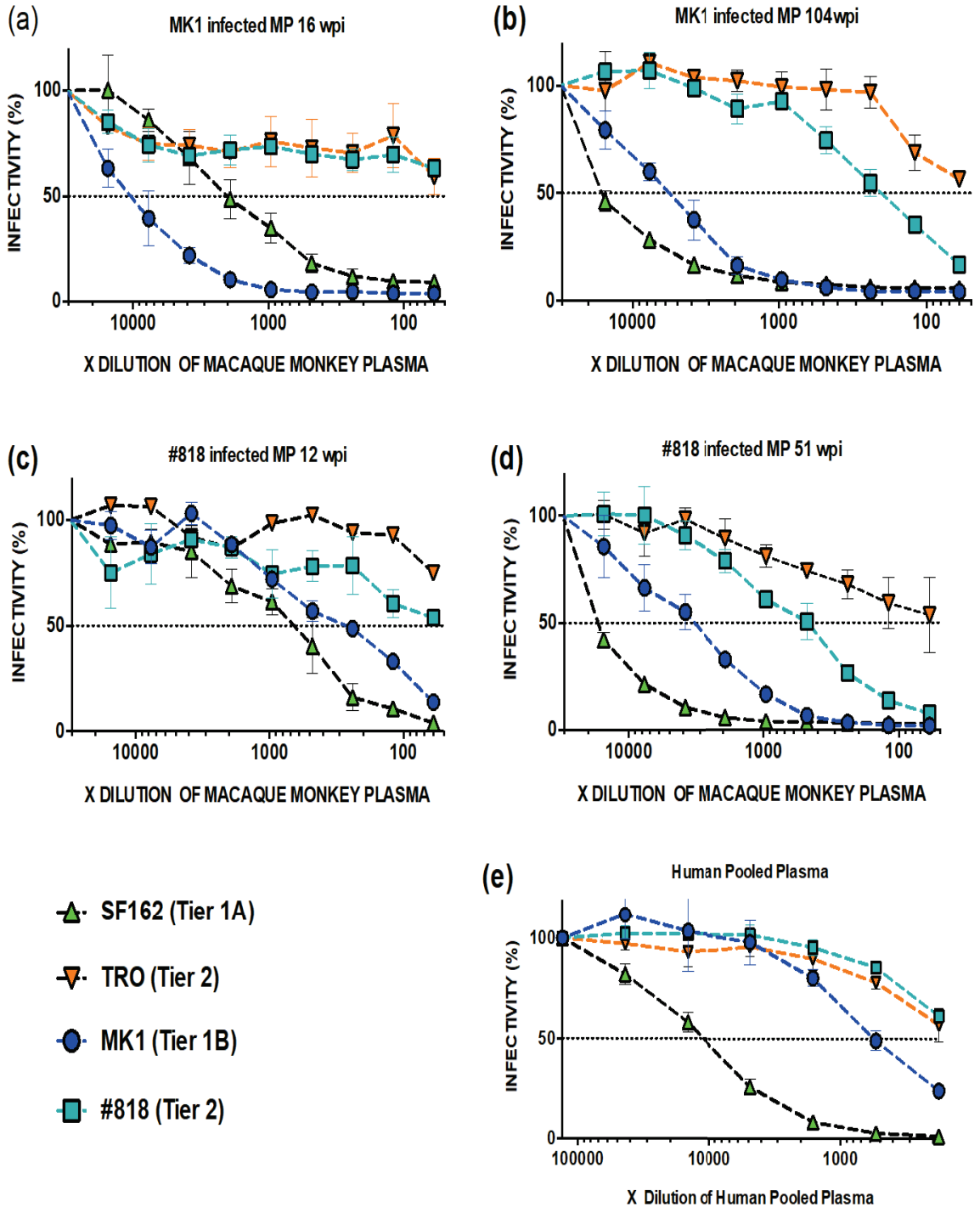

Analysis of the neutralisation resistance of each virus. (**a**–**d**) Neutralisation resistance of each virus to MM482 16 wpi, MM482 104 wpi, MM597 12 wpi, and MM597 51 wpi plasmas. After pre-incubating 100 $TCID_{50}$ of each virus and all MP samples, TZM-bl cells were

cultured with the mixture at 37 °C for 48 h and their luciferase activity was measured. All MP samples were diluted two-fold from 1:60 to 1:30,720. The values in parentheses are ID_{50}. (**e**) Neutralisation resistance of each virus to pooled plasma of HIV-1-infected individuals. After pre-incubating 100 $TCID_{50}$ of each virus and pooled plasma, TZM-bl cells were cultured with the mixture at 37 °C for 48 h and their luciferase activity was measured. Human pooled plasma was diluted three-fold from 1:180 to 1:13,1220. The values in parentheses are ID_{50}.

Figure 3.

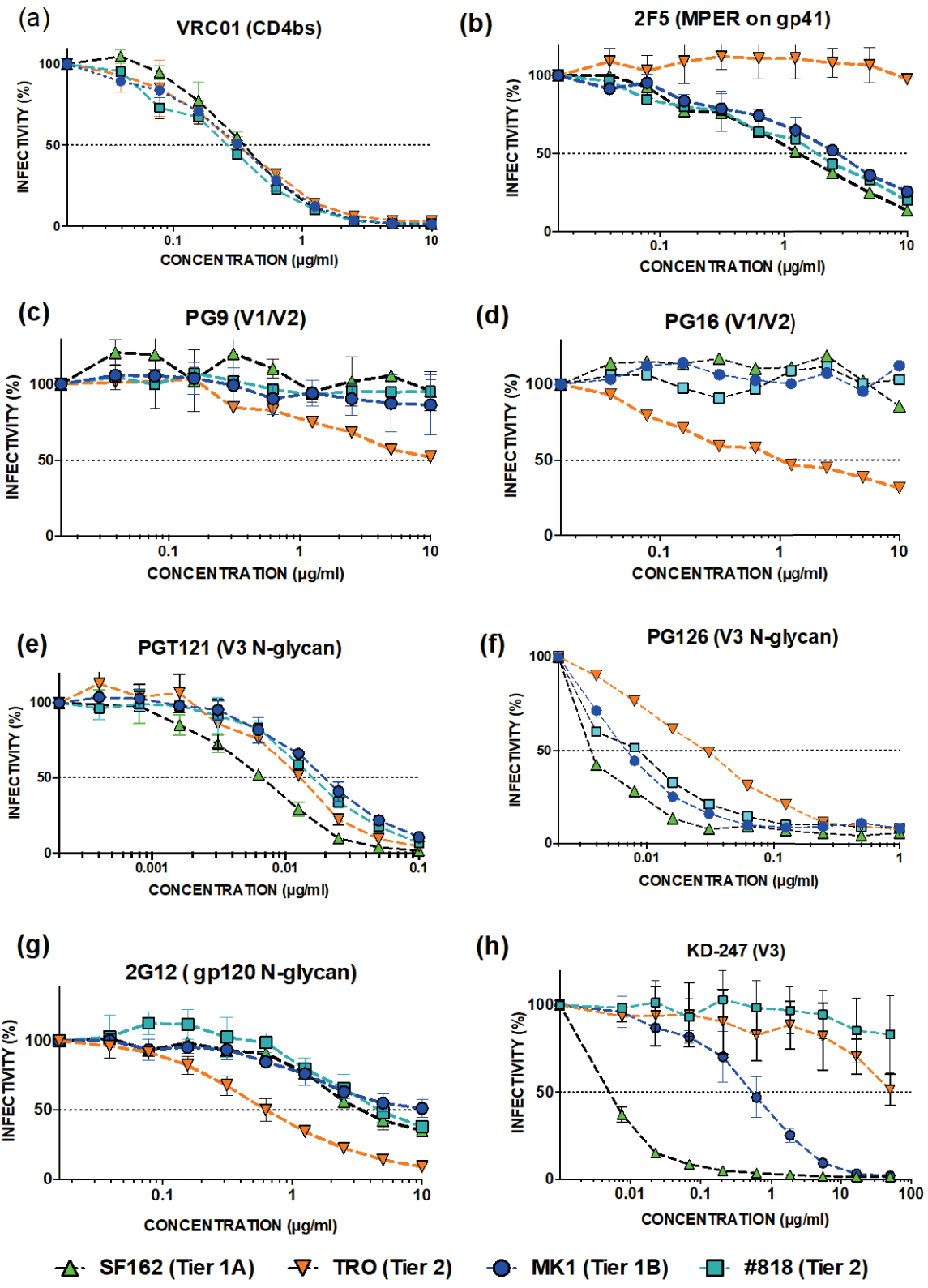
(a)
VRC01 (CD4bs)
(b)
2F5 (MPER on gp41)
(c)
PG9 (V1/V2)
(d)
PG16 (V1/V2)
(e)
PGT121 (V3 N-glycan)
(f)
PG126 (V3 N-glycan)
(g)
2G12 (gp120 N-glycan)
(h)
KD-247 (V3)
INFECTIVITY (%)
CONCENTRATION (µg/ml)
SF162 (Tier 1A)
TRO (Tier 2)
MK1 (Tier 1B)
#818 (Tier 2)

Analysis of the neutralisation resistance of each virus to eight anti-HIV-1 neutralising mAbs. After pre-incubating 100 $TCID_{50}$ of each virus and each HIV-1-neutralising mAb, TZM-bl cells were cultured with the mixture for 48 h, after which the luciferase activity was measured. (a) MAb VRC01 recognizes the structure that includes CD4bs on gp120 [7]. VRC01 was diluted two-fold from 10 to 0.02 µg/mL. (b) 2F5 is a recombinant monoclonal antibody to HIV-1 gp41 [8]. 2F5 was diluted two-fold from 10 to 0.02 µg/mL. (c) PG9 is a recombinant, broadly neutralizing monoclonal antibody (bnMAb) to HIV-1 gp120, specifically to quaternary structure of V1V2 [9]. PG9 was diluted two-fold from 10 to 0.02 µg/mL. (d) PG16 is a recombinant, bnMAb to HIV-1 gp120, specifically to the quaternary structure of V2 [9]. PG16 was diluted two-fold from 10 to 0.02 µg/mL. (e) PGT 121 is a recombinant, bnMAb to HIV-1 gp120, specifically to the N332-centered oligomannose patch on the V3 loop [10]. PGT121 was diluted two-fold from 0.1 to 0.0002 µg/mL. (f) PGT126 is a recombinant, bnMAb to HIV-1 gp120, specifically to the N332-centered oligomannose patch of the V3 loop. PGT 126 was diluted two-fold from 1 to 0.002 µg/mL [10]. (g) 2G12 is a recombinant mAb to HIV-1 gp120. 2g12 contact with gp120 carbohydrates at glycosylation residues in C2, C3, C4, V3 and V4, gp120 [11,12]. 2G12 was diluted two-fold from 10 to 0.02 µg/mL. (h) KD-247 binds PGR epitope on V3 region and efficiently neutralizes CXCR4- and CCR5-tropic primary HIV-1 clade B including tier 2 JR-CSF virus [13]. KD247 was diluted three-fold from 50 to 0.001 µg/mL.

Figure 4.

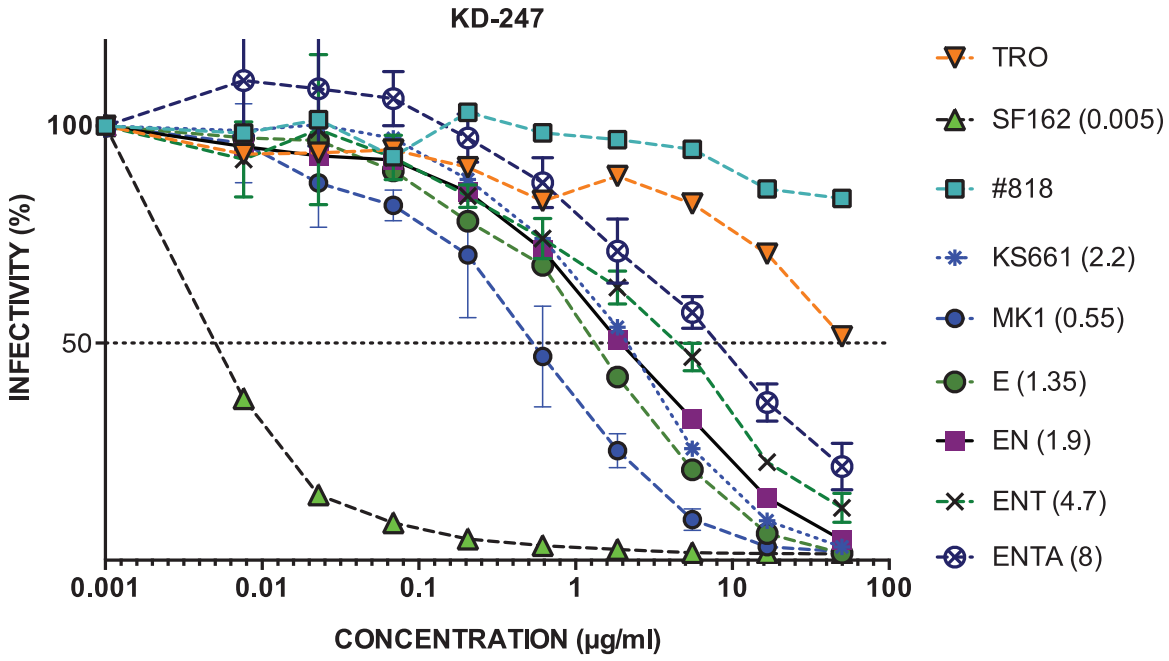

Analysis of the neutralisation resistance of each virus to anti-HIV-1 V3 KD247 Ab. After pre-incubating 100 $TCID_{50}$ of each virus and KD247 mAb, TZM-bl cells were cultured with the mixture for 48 h, after which the luciferase activity was measured. KD247 was diluted three-fold from 50 to 0.001 µg/mL. The values in parentheses are ID_{50}. The different viruses are as follows: E (MK1env K187E), EN (MK1env K187E, S190N), ENT (MK1env+K187E, S190N, A389T), and ENTA (MK1env K187E, S190N, A389T, T437A).

Figure 5.

(a)

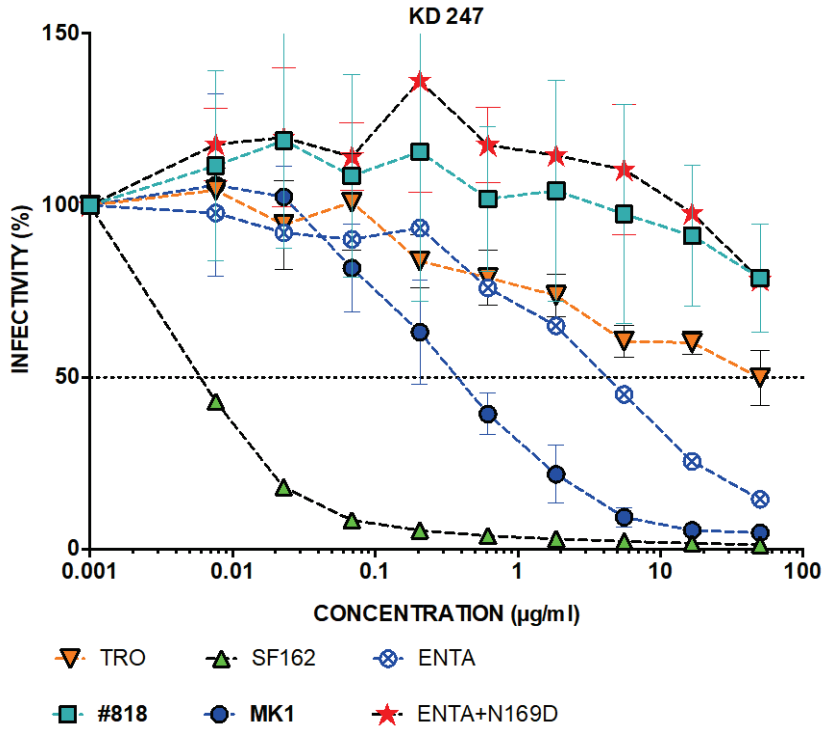
KD 247
150
100
50
0
INFECTIVITY (%)
0.001
0.01
0.1
1
10
100
CONCENTRATION (µg/ml)
TRO
SF162
ENTA
#818
MK1
ENTA+N169D

(b)

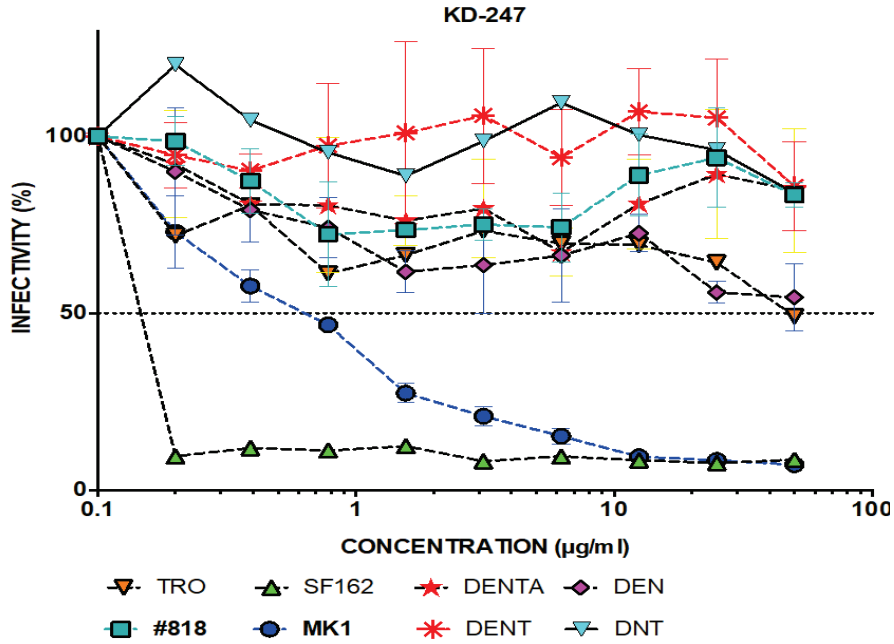
KD-247
100
50
0
INFECTIVITY (%)
0.1
1
10
100
CONCENTRATION (µg/ml)
TRO
SF162
DENTA
DEN
#818
MK1
DENT
DNT

(c)

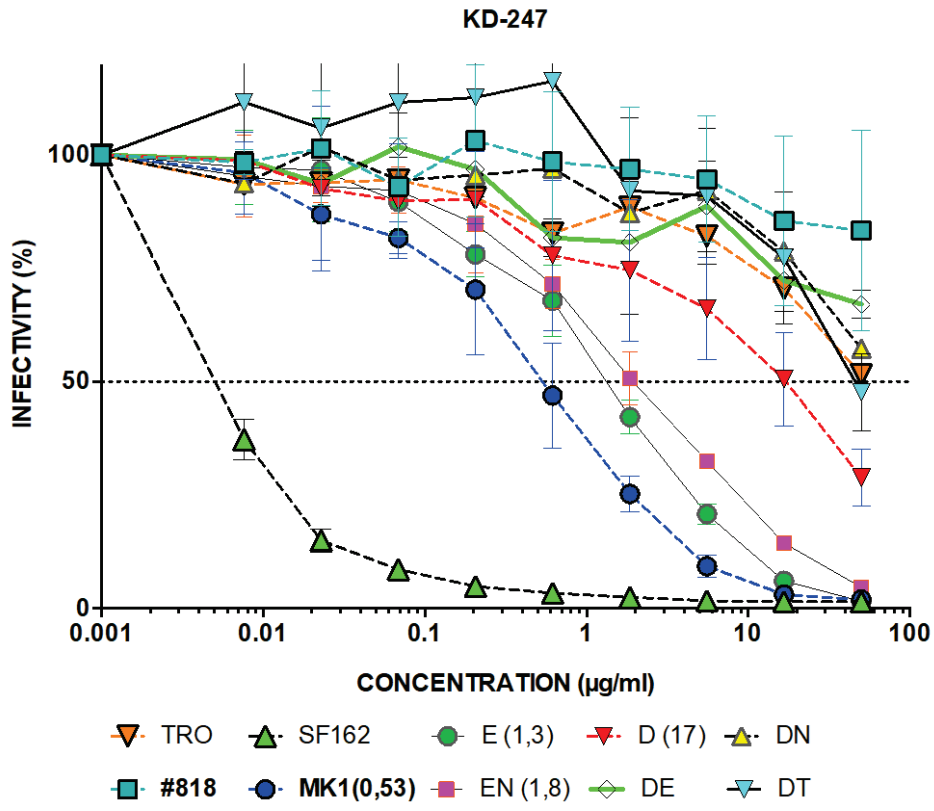

Analysis of the neutralisation resistance of each virus to anti-HIV-1 V3 KD247 mAb. After pre-incubating 100 $TCID_{50}$ of each virus with KD247 mAb, TZM-bl cells were cultured with the mixture for 48 h, after which the luciferase activity was measured. KD247 was diluted (**a**) three-fold from 50 to 0.01 µg/mL; (**b**) two-fold from 50 to 0.1 µg/mL; or (**c**) three-fold from 50 to 0.01 µg/mL. The different viruses are as follows: ENTA (MK1env K187E, S190N, A389T, T437A), DENTA (MK1env K187E, S190N, A389T, T437A+N169D), DENT (MK1env+K187E, S190N, A389T+N169D), DNT (MK1env+N169D, S190N, A389T), MK1+DEN (MK1env + N169D, K187E, S190N), DE (MK1env+N169D, K187E), DN (MK1env+N169D, S190N), DT (MK1env+N169D, A389T), DT (MK1env+N169D, A389T), D (MK1env+N169D), and E (MK1env+ K187E).

Figure 6.

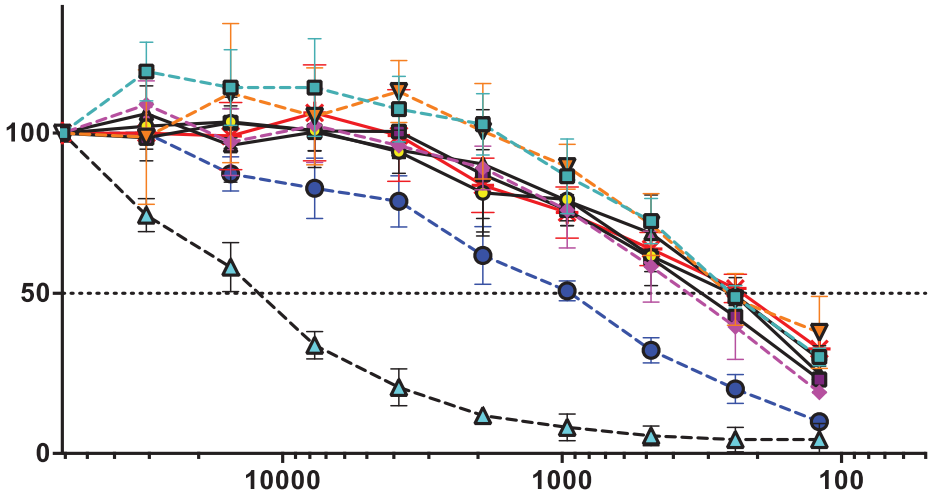

Neutralisation resistance of each virus to pooled plasma from HIV-1-infected individuals. After pre-incubating 100 $TCID_{50}$ of each virus and pooled plasma, TZM-bl cells were cultured with the mixture at 37 °C for 48 h and their luciferase activity was measured. HPP was diluted two-fold, from 1:120 to 1:61,440. The values in parentheses are ID_{50}. The different viruses are as follows: DENT (MK1env + N169D, K187E, S190N, A389T), DNT (MK1env + N169D, S190N, A389T), DEN (MK1env + N169D, K187E, S190N), DE (MK1env+ N169D, K187E), and DN (MK1env + N169D, S190N).

Figure 7.

(a)

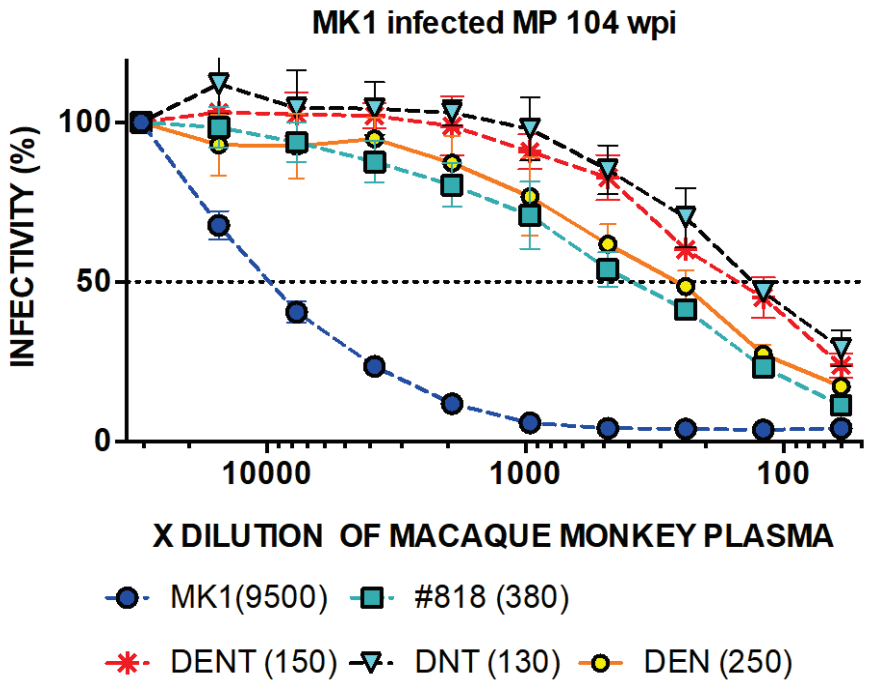
MK1 infected MP 104 wpi
INFECTIVITY (%)
100
50
0
10000
1000
100
X DILUTION OF MACAQUE MONKEY PLASMA
MK1(9500)
#818 (380)
DENT (150)
DNT (130)
DEN (250)

(b)

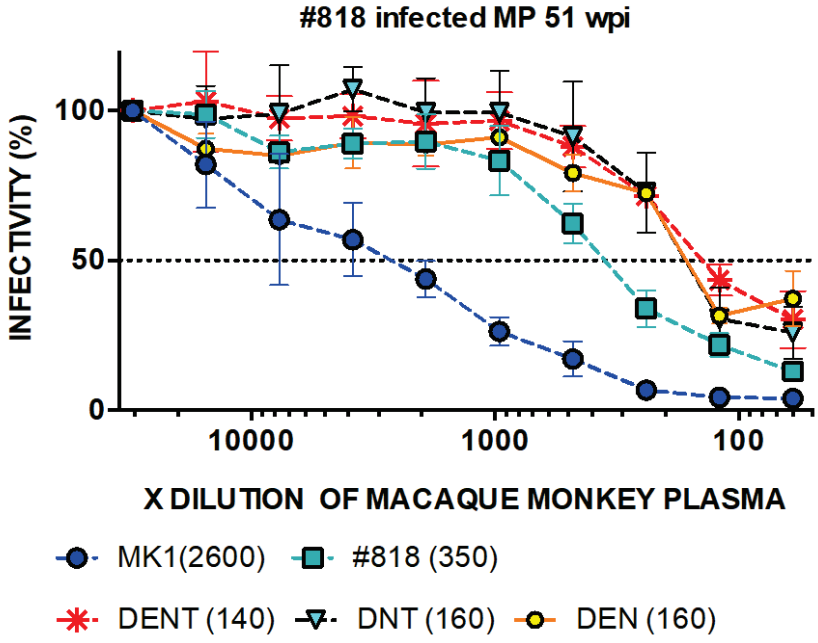
#818 infected MP 51 wpi
INFECTIVITY (%)
100
50
0
10000
1000
100
X DILUTION OF MACAQUE MONKEY PLASMA
MK1(2600)
#818 (350)
DENT (140)
DNT (160)
DEN (160)

Neutralisation resistance of each virus to MM482 104 wpi and MM597 51 wpi plasma (**a**,**b**). After pre-incubating 100 $TCID_{50}$ of each virus and all MP samples, TZM-bl cells were cultured with the mixture at 37ºC for 48 h and their luciferase activity was measured. All MP samples were diluted two-fold, from 1:60 to 1:30720. The values in parentheses are ID_{50}. The different viruses are as follows: DENT (MK1env + N169D, K187E, S190N, A389T), DNT (MK1env + N169D, S190N, A389T), and DEN (MK1env + N169D, K187E, S190N).

Figure 8.

(a)

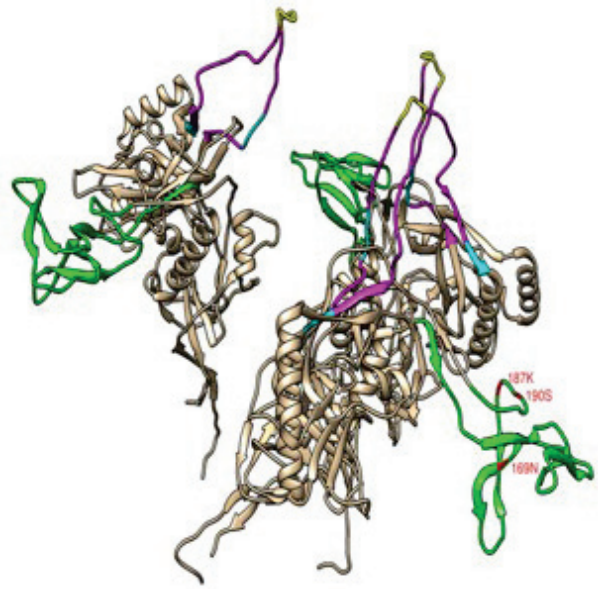

(b)

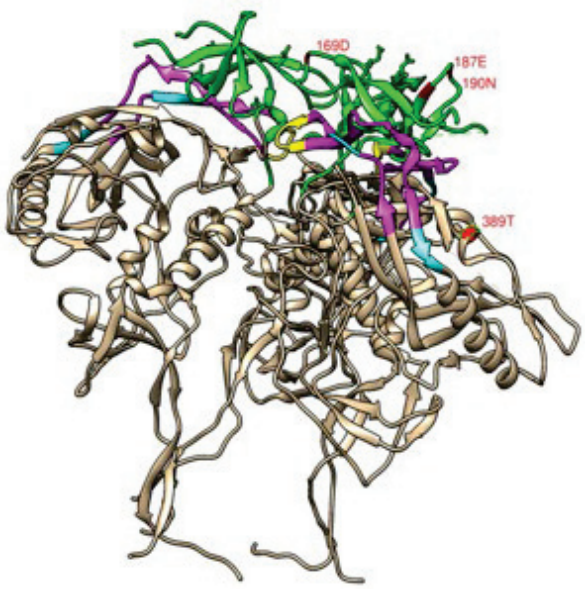

(c)

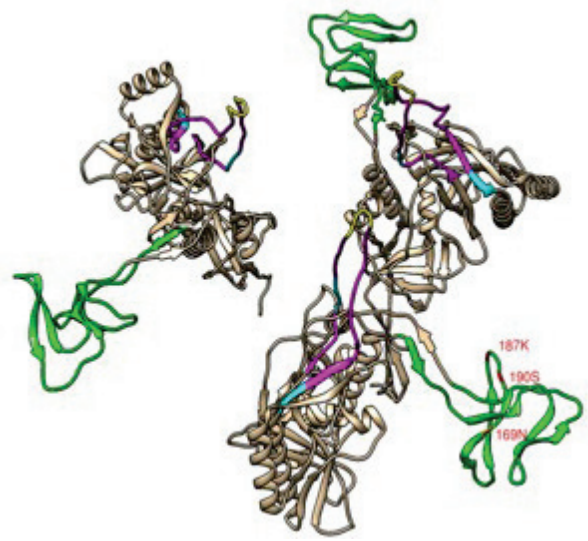

(d)

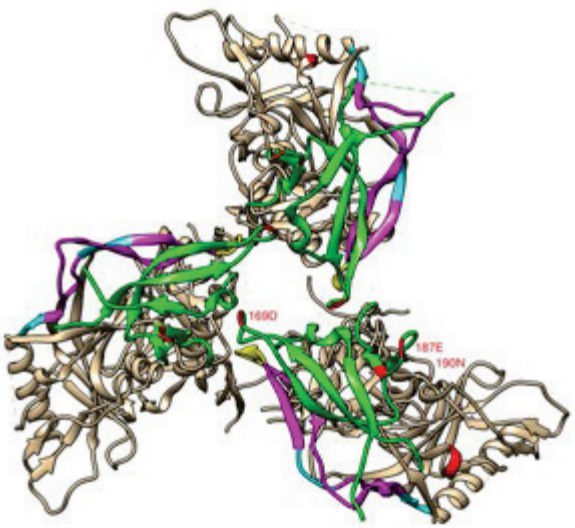

(e) **(f)**

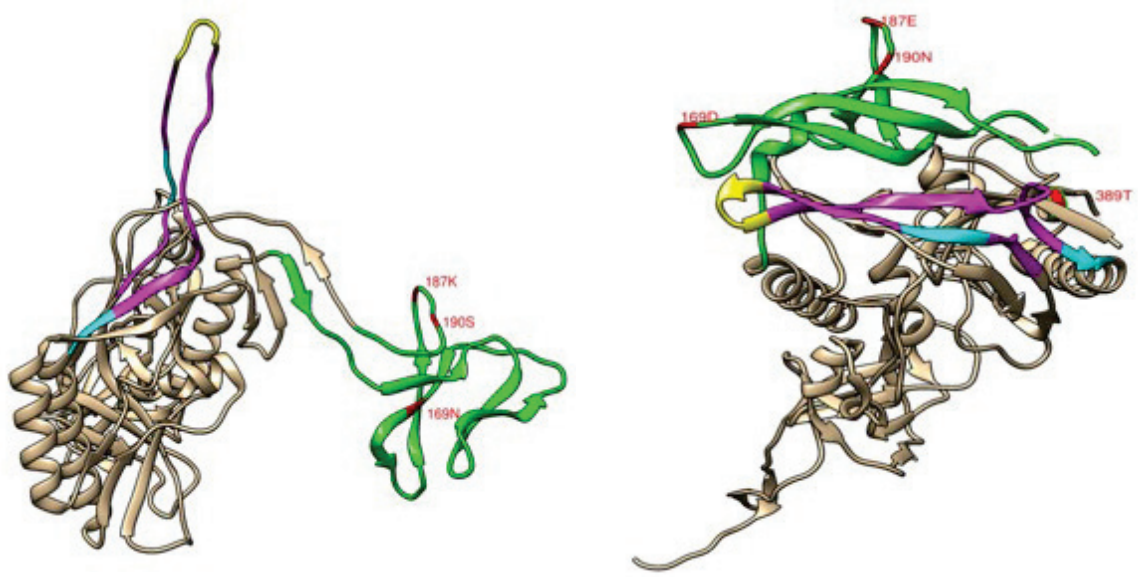

a) Model (side) of the gp120 trimeric structure of Env that mimics a tier 1 HIV (CD4 and 17b complexed with the full-length HXB2 HIV-1 Env).

(**b**) Model(side) of the gp120 trimeric structure of Env HIV (PGT145 Fab complexed with full-length AMC011 HIV-1 Env).

(c) Model (above) of the gp120 trimeric structure of Env that mimics a tier 1 HIV.

(**d**) Model (above) of the gp120 trimeric structure of Env HIV that mimics a tier 2 HIV.

(e) Model of the gp120 monomeric structure of Env that mimics a tier 1 HIV.

(**f**) Model of the gp120 monomeric structure of Env HIV that mimics a tier 2 HIV.

The four most important amino acid bases associated with MK1 (**a**)(c)(e) and MK38#818 (**b**)(d)(f) are labelled in red. The models are from Protein Data Bank ID: 3J70 and 6NIJ, respectively, and were visualised using UCSF Chimera software [23,24] Both models show the V1/V2 (green) and V3 (magenta) domains and KD247 (yellow) and PGT121 (cyan) epitopes.

Chapter 3.

The Neutralization Assay of Pseudo-Typed Lentivirus SARS CoV-2 Spike on ACE2 expressing CRFK Cell

3.1. Abstract

Severe acute respiratory syndrome coronavirus 2 (SARS-CoV-2) is highly pathogenic zoonotic virus and spread rapidly, with more deaths. In this work, we improve to hitherto existing neutralization assay system to assess SARS-CoV-2 inhibitors using a pseudo-typed lentivirus coated with the SARS-CoV-2 spike protein (LpVspike +) and ACE2-transfected cat CRFK cells as the host cell line. Our method was 10-fold more sensitive compared to the typical HEK293T cell system, and it was successfully applied to quantify the titres of convalescent antisera and monoclonal anti-spike antibodies required for pseudo virus neutralization. The ID50 of two human convalescent sera, SARS-CoV-2 IgG and SARS-CoV-2 IgM, which were 1:350(± 1:20) and 1:1250(± 1:350), respectively. The IC50 of the IgG, IgM and IgA anti-SARS-CoV-2 mAbs against LpVspike(+) were 0.45 (±0,1), 0.002 (±0,001) and 0.004 (±0.001) μg mL^{-1}, respectively. We also found that reagents typically used to enhance infection were not effective in the CFRK system. This methodology is both efficient and safe; it can be employed by researchers to evaluate neutralizing monoclonal antibodies and contribute to the discovery of new antiviral inhibitors against SARS-CoV-2.

3.2. Introduction

An outbreak of severe acute respiratory syndrome (SARS) from 2002–2003 in Guangdong, China resulted in over 8,000 infections and almost 800 deaths. This was caused by a coronavirus (CoV), known as SARS-associated CoV (SARS-CoV) [78]. In December 2019, a novel infectious disease caused by a related coronavirus, SARS-CoV-2, was reported in Wuhan, China, and is widely referred to as coronavirus disease 2019 (COVID-19) [79]. SARS-CoV-2 belongs to the same species as SARS-CoV and other SARS-related bat CoVs [80]. COVID-19 has been declared a worldwide pandemic by the World Health Organisation (WHO) and has so far infected over 51 million people and killed more than 1.2 million.

SARS-CoV-2 is a β-coronavirus, as characterized by its envelope and non-segmented, positive-sense single-stranded RNA genome [81]. It has a genome size of 29,881 bp, which encode 9,860 amino acids [82]. Two-thirds of the viral RNA encodes two polyproteins and 16 non-structural proteins, whereas the remainder of the viral genome encodes four essential structural proteins: the spike (S) glycoprotein, a small envelope protein, a matrix protein and a nucleocapsid protein. Several accessory proteins, which interfere with the host innate immune response, are also encoded within the viral genome [81, 83, 84].

The S protein is 1,273 amino acids in length and is coated with polysaccharide molecules, providing camouflage that enables the virus to evade the host immune system during entry [85]. During its biosynthesis, the S protein is cleaved by a furin-like protease in the Golgi apparatus into two subunits, S1 and S2, which form the bulbous head and stalk regions of the S protein. The S proteins of both SARS-CoV-2 and SARS-CoV bind to the angiotensin-converting enzyme 2 (ACE2) receptor, which they use for cell entry [78, 86, 87]. Following binding of the S protein to the ACE2 receptor, transmembrane protease serine 2 (TMPRSS2), which is located on the host

cell membrane, further cleaves the S2 subunit into S2` and S2`` subunits, activating the membrane fusion domain [88].

Vero and VeroE6 cells, which express the ACE2 receptor at high levels, have been used to isolate and study SARS-CoV-2. SARS-CoV-2 is categorized as a biosecurity level (BSL) 3 agent according to WHO guidelines, which impedes the rapid development of new protocols and medicines related to the virus [89-91]. To lower the biosecurity risk of viruses, non-replicative pseudo-typed viruses carrying viral S proteins on their surfaces have been developed; these pseudoviruses can infect host cells but cannot replicate, meaning that they can be dealt with using less stringent BSL-2 facilities [92]. Pseudoviruses have recently been developed for SARS-CoV-2 using human immunodeficiency virus (HIV)-based lentiviral particles, murine leukaemia virus-based retroviral particles and the vesicular stomatitis virus (VSV) [92]. VSV pseudo-types expressing the SARS-CoV-2 S protein are currently being used to study viral entry [86]; however, the construction of VSV-based pseudo-typed viruses requires a complex procedure. By contrast, pseudo-typed lentiviral viruses can be produced using a comparatively simple method, involving the co-transfection of host cells with multiple plasmids [87]. Human embryonic kidney 293T (HEK293T) cells are currently the main cell line used for the production of pseudo-typed SARS-CoV-2 and to assay its infectivity due to its high transfection efficiency. However, further improvements to this system could be made [80].

Here, we report the development of a simple assay that is 10-fold more sensitive than the commonly-used HEK293T cell assay, using a pseudo-typed lentivirus coated with SARS-CoV-2 S protein (LpVspike [+]). Using our system, we successfully measured the titre of anti-CoV antibodies required for neutralization. Figure 1 shows an illustration outlining our new system.

3.3. Results

3.3.1. Measuring LpVspike (+) infectivity in various ACE2-expressing cell types

Although ACE2-expressing HEK293T cells are typically used with the pseudo-typed lentiviral system, the sensitivity of infectivity assays is low. With the goal of identifying a more sensitive cell line, we measured the infectivity of a SARS-CoV-2-S-coated pseudovirus, or LpVspike(+), in the following ACE2-expressing cell lines: Cos7, TZM-bl, Crandell-Rees feline kidney (CRFK) and Vero cells. The various cell types were infected with 100 µL of viral solution in 96-well plates. The luciferase readings, which indicated pseudoviral infection, were > 10-fold higher in ACE2-expressing CRFK (ACE2-CRFK) cells compared to ACE2-expressing HEK293T (ACE2-HEK293T) cells; ACE2-CRFK cells and ACE2-HEK293T cells produced readings of 8×10^4 and 5×10^3 relative luciferase units (RLU), respectively. A reading of approximately 5 RLU was detected in uninfected control cells (Figure 2).

We also examined LpVspike(+) infectivity in VeroE6/TMPRSS2 cells, which have previously been shown to be 10-fold more sensitive to infection than parental VeroE6 cells [93]. LpVspike(+) infected VeroE6/TMPRSS2 cells less efficiently compared to ACE2-CRFK and ACE2-HEK293T cells (Figure 2). A reading of only 10^3 RLU was detected when VeroE6/TMPRSS2 cells were infected with 100 µL of viral solution. LpVspike(+) did not appear to infect ACE2-expressing Cos7 cells (Figure 2).

The TZM-bl cell line (also called JC.53bl-13) is a HeLa cell derivative engineered to express CD4, CCR5 and CXCR4, as well as Tat-responsive firefly luciferase reporter genes. These features make TZM-bl cells highly susceptible to HIV-1 infection and enables quantification of viral infection and neutralizing antibody titres [94]. Because TZM-bl already has an integrated copy of the luciferase reporter gene, we constructed a second pseudo-typed lentivirus, named

LpVspike2(+); this was essentially the same as LpVspike(+), except it did not contain the luciferase gene. ACE2-expressing TZM-bl cells infected with undiluted LpVspike2(+) produced a reading of 2×10^4 RLU, which was comparable to that of the background cell line that had not been virally infected (1×10^4 RLU; Figure 2). Therefore, the TZM-bl cell line was deemed an unsuitable host for our S-covered pseudo-typed lentivirus system.

3.3.2. The comparison of LpVspike(+) infectivity in HEK293T and CRFK cell lines with/without ACE2 transfection

The S protein of SARS-CoV-2 uses ACE2 as its point of entry, and hence requires host ACE2 expression to initiate infection. We confirmed the specificity of this process by examining the infectivity of pseudo-typed lentiviruses containing the SARS-CoV-2 S protein (LpVspike[+]) and those that did not (LpVspike[−]) in four cell lines: CRFK, ACE2-CRFK, HEK293T and ACE2-HEK293T. Neither LpVspike(+) nor LpVspike(−) infected the HEK293T cells. LpVspike(+) and a small amount of LpVspike(−) were able to infect ACE2-HEK293T cells, with LpVspike(+)- and LpVspike(−)-infected ACE2-HEK293T cells producing readings of 2,000 and 500 RLU with 50 μL of viral solution, respectively (Figure 3a). These results suggest that LpVspike(−) can infect ACE2-HEK293T cells non-specifically, without binding to the ACE2 receptor.

Neither LpVspike(+) nor LpVspike(−) infected CRFK cells. Whereas LpVspike(+) infected ACE2-CRFK cells (10^4 RLU with 50 μL of viral solution), LpVspike(−) did not (Figure 3b). These results indicate that only LpVspike(+) can infect ACE2-transfected CRFK cells, indicating a S-ACE2 specific interaction.

3.3.3. Effect of diethylaminoethyl-dextran on infectivity

TZM-bl cells are maximally sensitive to HIV infection in diethylaminoethyl-dextran (Deax)-supplemented medium [94]. We therefore examined the effects of Deax on LpVspike(+) and LpVspike(−) infectivity in CRFK and ACE2-CRFK cells. Both LpVspike(+) and LpVspike(−) infected the CRFK cells in the presence of Deax, producing readings of 10^4–10^5 RLU per 50 μL of viral solution (Figure 4a); this was in contrast to CRFK cells without Deax, which were only infected by LpVspike(+). The ACE2-CRFK cells were infected by both LpVspike(+) and LpVspike(−) in the presence of Deax, whereas infection only occurred in the ACE2-CRFK line with LpVspike(+) infection (1×10^4 RLU with 50 μL of viral solution) in the absence of Deax. Deax can therefore induce non-specific LpVspike infection in CRFK cells. Notably, only LpVspike(+) efficiently infected ACE2-CRFK cells, LpVspike(−) could not infect CRFK or ACE2-CRFK cells without Deax (Figure 4b).

The addition of Deax increased the infection efficiency of both LpVspike(+) and LpVspike(−) 1,000-fold in CRFK cells. While Deax increased the infection efficiency of LpVspike(+) 10-fold in ACE2-CRFK cells, it increased the infection efficiency of LpVspike(−) 1,000-fold. These results suggest that Deax can cause non-specific infections in HEK293T, ACE2-HEK293T, CRFK and ACE2-CRFK cell lines. Deax was therefore ruled out as a supplement for enhancing LpVspike infection efficiency for our system.

3.3.4. Effect of polybrene on infectivity

Hexadimethrine bromide, also known as polybrene, is a cationic polymer capable of enhancing *in vitro* HIV-1 infection by reducing electrostatic repulsion between virions and sialic acid on the cell surface [95]. Polybrene has been widely used in neutralization and infectivity assays examining HIV and pseudo-typed lentiviruses coated with the SARS-CoV-2 S protein [78, 92, 96, 97]. Therefore, we examined the effect of polybrene in our pseudovirus system. Following LpVspike(+) infection, ACE2-CRFK cells produced a reading of approximately 10^4 RLU with 50 µL of viral solution both with and without polybrene supplementation, suggesting that polybrene did not provide any enhancement effect (Figure 5b). For both CRFK and ACE2-CRFK cells, no LpVspike(−) infection was detected following polybrene addition (Figure 5a, b). Therefore, polybrene did not induce non-specific infections.

3.3.5. Stability of ACE2 expression in CRFK cells and LpVspike(+)

We found that CRFK cells were the most sensitive of the cell lines tested, producing a 10-fold higher RLU reading compared to the HEK293T cells. In this experiment, ACE2 was expressed in CRFK cells using a transient system, as opposed to a stable genome-integrated system. We therefore set out to determine the stability of transient ACE2 expression in CRFK cells, with the goal of optimizing transfection conditions. Following seeding and harvesting, ACE2-transfected CRFK cells were incubated for three time periods: 1 h, 1 day and 2 days. At each time point, the ACE2-transfected CRFK cells were exposed to LpVspike(+) in 96-well plates, then incubated for a further 48 h. The luciferase reporter measurements were similar for each time point, suggesting that the CRFK cells stably express the ACE2 receptor throughout the 48-h period following transfection with the ACE2 vector (Figure 6a).

We then examined the stability of LpVspike(+) following incubation at 37 °C. After 1 h of incubation, luciferase expression had not changed, indicating that LpVspike(+) was stable (Figure 6b).

3.3.6. Inhibition of LpVspike(+) in ACE2-expressing CRFK cells with plasma and monoclonal antibodies

We next assessed whether our LpVspike(+)/ACE2-CRFK cell system could be applied to assess antibody neutralization. We first calculated the 50 % inhibition dilution (ID50) of two human convalescent sera, SARS-CoV-2 IgG and SARS-CoV-2 IgM, which were 1:350(± 1:20) and 1:1250(± 1:350), respectively (Figure 7). The luciferase readings at ID50 of LpVspike(+) against IgM and IgG were both approximately 1×10^4 RLU (Figure 7a).

Next, we examined the effect of monoclonal antibodies (mAbs) raised against SARS-CoV-2. The IC50 of the IgG, IgM and IgA anti-SARS-CoV-2 mAbs against LpVspike(+) were 0.45 (±0,1), 0.002 (±0,001) and 0.004 (±0.001) μg mL^{-1}, respectively (Figure 8b). Each of the anti-SARS-CoV-2 mAbs was able to neutralize pseudo-typed lentiviruses coated with SARS-CoV-2 S protein during the infection of ACE2-expressing CRFK cells (Figure 8a, b).

3.4. Discussion

In this study, we found that feline CRFK cells were 10-fold more sensitive to infection with S protein-coated HIV-1 pseudoviruses compared to human HEK293T cells. Given that both pseudoviral S-protein expression and CRFK ACE2 expression were required for infection with LpVspike(+), we conclude that our system reflects the natural SARS-CoV-2 infection process. Moreover, this system was tested by measuring the neutralizing activities of convalescent sera and anti-spike mAbs, thus demonstrating its practicality.

In contrast to the high LpVspike(+) infectivity observed in CRFK cells, the infection rates of Cos7 and Vero cells, which are derived from macaque kidneys, were low. The LpVspike(+) pseudovirus was based on HIV-1, meaning that completion of the infection process following entry into the cytoplasm is dependent on whether the host cellular environment facilitates viral uncoating, reverse transcription, movement of the virus into the nucleus, and integration of the viral genome into chromosomes. Macaque cells possess restriction proteins such as APOBEC3 and TRIM5α/TRIM5CypA, which disrupt the HIV-1 genome and core [98], whereas cat cells express a truncated, non-functional version of Trim5α. CRFK cells may lack both functional APOBEC3 and Trim5α. Although human APOBC3 and Trim5α cannot prevent HIV-1 infection, human Trim5α exhibits weak restriction activity [99].

Our attempts to improve infection efficiency by adding Deax and polybrene were not successful. Deax caused non-specific infection in all combinations of cell types and pseudoviruses tested, regardless of the presence of the S protein or its ACE2 receptor. However, Deax specifically enhanced the infection of TZM-bl cells expressing human CD4/CCR5 with a HIV-1 envelope-coated pseudovirus. Although we do not have a definitive explanation for these results, we propose that Deax may disturb the membranes of both the cell and virus. Another unexpected result is that

LpVspike(−) infected ACE2-HEK293T cells, but not ACE2-CRFK cells. ACE2 transfection might therefore perturb the membranes of HEK293T cells, causing non-specific infection.

The neutralization assay developed in this work using modified cat CRFK cells is an efficient and safe method that could be a useful research tool, enabling the examination of the binding mechanism between the SARS-CoV-2 S protein and the ACE2 receptor, as well as the development of antiviral drugs. As demonstrated above (Figure 8), this system could be employed to assess SARS-CoV-2 inhibitors and evaluate the neutralizing activity of convalescent antisera and anti-S protein mAbs; anti-S protein antibodies may be useful in treating critically ill COVID-19 patients. Although vaccine development is progressing at an unprecedented rate, this neutralization assay could still be a useful tool for determining the robustness of the B-cell response elicited by newly developed SARS-CoV-2 vaccines.

3.5. Materials and Methods

3.5.1. Cell culture

HEK293T cells (American Type Culture Collection [ATCC] CRL 3216), CRFK cells (ATCC CCL-94), African green monkey kidney clone of Vero-E6 (VeroE6) cells (ATCC CRL 1586), monkey kidney fibroblast-like cell lines (Cos7; ATCC CRL 1651) and TZM-bl cells (National Institute of Allergy and Infectious Diseases [NIH] ARP #8129) were cultured in Dulbecco's modified Eagle's medium (DMEM) (Fujifilm Wako Pure Chemical Corporation, Osaka, Japan) supplemented with 10 % (v/v) heat-inactivated foetal bovine serum, 2 mM sodium pyruvate (MP Biomedicals Inc., Santa Ana, CA, USA) and 4 mM L-glutamine (Fujifilm Wako Pure Chemical Corporation). Cells were harvested and passaged using trypsin/ ethylenediaminetetraacetic acid solution (Nacalai Tesque, Kyoto, Japan). All cell lines were maintained at 37 °C under 5 % CO_2 in a humidified environment.

3.5.2. Generation of pseudo-typed lentivirus with SARS-CoV-2 S particles

Cloning of all DNA plasmids was conducted by transformation into *Escherichia coli* Stbl3 cells as described previously [100]. Lentiviral-based pseudo-type viruses were constructed as described previously [101]. In brief, pseudo-type lentiviruses coated with the SARS-CoV-2 S protein harbouring the vector 2019-nCov_pcDNA3.1(+)-P2A-eGFP spike (1 μg mL^{-1}) were prepared by co-transfecting 5×10^5 cells mL^{-1} of HEK293T cells with the HIV-1 NL4-3 ΔEnvΔ Vpr Luciferase Reporter Vector (1 μg mL^{-1}) [102].

Additionally, 200 μL of OptiMem and 8 μL of X-treme HP transfection reagent were added. Transfected HEK293T cells were incubated at 37 °C under 5 % CO_2 for 2 days, after which the supernatant containing pseudo-typed lentivirus particles coated with SARS-CoV-2 S protein was

harvested and filtered through a 0.45-µm filter (Millipore, Burlington, MA, USA); 400-µL aliquots were stored in 1.5-mL tubes at –80 °C. The 1 µg mL^{-1} HIV-1 NL4-3 ΔEnv Vpr Luciferase Reporter Vector (pNL4-3. Luc. R-E-) (catalogue number 3418) was kindly provided by Dr Nathaniel Landau (NIH AIDS Reagent Program, Division of AIDS). The 2019-nCov_pcDNA3.1(+)-P2A-eGFP spike vector (catalogue number MC_0101087) was purchased from Nacalai Tesque from Molecular Cloud.

Pseudo-typed lentiviruses with SARS-CoV-2 S protein without the luciferase gene were also constructed to transfect the TZM-bl cell line. Pseudo-type lentivirus particles coated with SARS-CoV-2 S that harboured the 2019-nCov pcDNA3.1 plasmid (1 µg mL^{-1}) or 2019-nCoV pCMV plasmid (1 µg mL^{-1}) were generated by co-transfecting HEK293T cells with the pSGΔenv vector (1 µg mL^{-1}). The pSGΔenv (catalogue number 11051) vector was kindly provided by Dr. John C. Kappes and Dr. Xiaoyun Wu (NIH AIDS Reagent Program, Division of AIDS).

3.5.3. Generation of transient ACE2-expressing cell lines

HEK293T, CRFK, Cos 7 and TZM-bl cells were seeded at concentrations of 2.5×10^5 cells mL^{-1} in six-well plates, using DMEM supplemented with 10 % foetal bovine serum, 2 % L-glutamine and 2 % pyruvate. Cell lines were incubated for 1 day, at which point cell confluency reached 60–80 %. The pcDNA3.1+/C-(K) DYK-ACE2 (2 µg mL^{-1}) plasmid was transfected into the cell lines with 200 µL of OptiMem and 8 µL of X-treme HP transfection reagent. The pcDNA3.1+/C-(K) DYK-ACE2 plasmid (catalogue number MC_0101086) was purchased from Nacalai Tesque (Molecular Cloud). ACE2-expressing cell lines were seeded at a cell concentration of 2.5×10^5 cells mL^{-1} in six-well plates and incubated at 37 °C under 5 % CO_2 for 1 day. HEK293T cells were seeded in poly-L-lysine-coated 96-well plates (Sumitomo Bakelite Celltight Poly-L-

lysine-coated flat bottom 96-well plates, catalogue no: ms-0096L). All other cell types were seeded in standard 96-well plates (Falcon tissue culture plate, 96 wells, flat bottom with low evaporation lid, ref 353072).

3.5.4. Neutralization assays

ACE2-expressing CRFK cells were seeded into 100 µL of medium to a concentration of 2.5×10^5 cell mL^{-1} in 96-well plates 1 day before infection. Previously harvested samples containing pseudo-typed lentiviral particles coated with the SARS-CoV-2 S protein were thawed. To perform the virus titration, pseudo-typed virus samples were serially diluted two-fold a total of nine times and transferred to a 96-well plate. Control wells contained only supplemented medium and no virus sample. Each dilution was made in triplicate. For infection, 100 µL of each LpVspike(+) or LpVspike2(+) dilution was added to the cell-seeded 96-well plates, which were incubated at 37 °C under 5 % CO_2 for 2 days.

Luciferase activity was measured in HEK293T, CRFK, Cos7, Vero and TZM-bl cells [Wei, 2002]. The details of the neutralization assays performed in this study have been described previously [103, 104]. Briefly, to measure luciferase activity, 50 µL of cell lysate solution (Toyo B-Net, Tokyo, Japan) was added to each well, and the plate was agitated for 15 min. An aliquot of 30 µL of lysate was transferred to a Nunc F96 MicroWell white plate (Thermo Fisher Scientific, Waltham, MA, USA), and luminescent substrate (30 µL) was added to each well. Luciferase activity was measured using a TriStar LB 941 reader (Berthold Technologies, Bad Wildbad, Germany) and MikroWin software. ID50 values were calculated as previously described [34].

The neutralization assays were performed using adjusted viral doses that yielded equivalent infectivity levels for each cell line. The neutralization assays were performed in a 96-well format

as described previously; ID50 was reported as either the concentration or sample dilution at which the RLU readout was reduced by 50 % compared to the RLU readings measured in the virus control wells (cells plus virus without test sample) after subtracting background RLU values from cell control wells (cells only, no virus or test sample) [105].

To test the stability of ACE2-expression in CRFK cells, ACE2-expressing CRFK cells were seeded to a concentration of 2.5×10^5 mL^{-1} in 96-well plates and incubated for three different time periods: 1 h, 1 day and 2 days. Pseudo-typed viruses were then added to a final concentration of 6,000 RLU mL^{-1} to the ACE2-expressing CRFK cells and incubated for 48 h at 37 °C under 5 % CO_2.

To evaluate the stability of LpVspike(+) when incubating at 37 °C, diluted pseudo-typed viruses were incubated in triplicate for 10, 30 and 60 min. To test viral infectivity after incubation at 37 °C, virus samples were added to ACE2-expressing CRFK cells in 96-well plates and incubated for 48 h at 37 °C under 5 % CO_2.

SARS-CoV-2 plasma serum of COVID-19 patients with varying IgM and IgG antibody levels was purchased from RayBiotech (Peachtree Corners, GA, USA). The serum plasma was subjected to serial three-fold dilutions, from an initial dilution of 1:60 down to 1:1,180,980. We added 120 µL of supplemented medium to each well in a 96-well plate, with the exception of the outer edge wells, to which 250 µL of phosphate-buffered saline was added. Next, 180 µL of 1/20- or 1/40-diluted plasma was added to the first row of wells and subjected to three-fold serial dilutions. Control wells contained no plasma, only cells and virus. Then, 60 µL of pseudo-typed virus at a concentration of 6000 RLU mL^{-1} was added to wells containing the diluted plasma. The total volume of the diluted plasma and virus was approximately 180 µL. The plasma-virus mixtures were incubated at 37 °C under 5 % CO_2 for 1 h. After incubation, 150 µL of the mixture was added

to the seeded ACE2-expressing CRFK cells in 96-well plates. The plates were incubated at 37 °C under 5 % CO_2 for 2 days, then the luciferase activity of the samples was measured. ID50 was calculated as described previously [34].

Three anti-SARS-CoV-2 neutralizing mAbs were used, including IgG, IgM and IgA. The mAbs were diluted 10-fold three times from 1 to 0.001 μg mL^{-1}. The experimental method for testing neutralizing mAbs was the same as the method used for assessing the neutralizing ability of plasma. IC50 values were calculated as described previously [34]. Anti-2019-nCoV S-hIgG1 Neutralizing antibody (catalogue number E-AB-V1021), Anti-2019-nCoV S-IgM Neutralizing antibody (catalogue number E-AB-V1026) and Anti-2019-nCoV S-IgA Neutralizing antibody (catalogue number E-AB-V1027) were purchased from Elabscience (Houston, TX, USA).

3.6. Conclusion

ACE2-expressing CRFK cells were 10 times more sensitive to viral infection compared to the typically used HEK293T cells. We tested our system with a neutralization assay and found that the pseudo-typed lentiviruses coated with SARS-CoV-2 S protein were neutralized by anti-SARS-CoV-2 IgG, IgM and IgA mAbs and sera. We also evaluated the influence of Deax and polybrene on infectivity; Deax caused non-specific viral infection in the absence of ACE2 receptors, and polybrene did not have a significant impact on infectivity or sensitivity. Our neutralization assay using pseudo-typed lentiviruses coated with SARS-CoV-2 S protein and ACE2-expressing CRFK cells is both easier and safer than the methods currently available and can aid researchers in understanding SARS-CoV-2 pathogenesis as well as discovering new drugs and vaccines.

3.7. References

1. Ren, W., et al., *Difference in receptor usage between severe acute respiratory syndrome (SARS) coronavirus and SARS-like coronavirus of bat origin.* J Virol, 2008. 82(4): p. 1899-1907.
2. Zhu, N., et al., *A Novel Coronavirus from Patients with Pneumonia in China, 2019.* N Engl J Med, 2020. 382(8): p. 727-733.
3. Harcourt, J., et al., *Isolation and characterization of SARS-CoV-2 from the first US COVID-19 patient.* bioRxiv, 2020.
4. Guo, Y.R., et al., *The origin, transmission and clinical therapies on coronavirus disease 2019 (COVID-19) outbreak - an update on the status.* Mil Med Res, 2020. 7(1): p. 11.
5. Khailany, R.A., M. Safdar, and M. Ozaslan, *Genomic characterization of a novel SARS-CoV-2.* Gene Rep, 2020. 19: p. 100682.
6. Narayanan, K., C. Huang, and S. Makino, *SARS coronavirus accessory proteins.* Virus Res, 2008. 133(1): p. 113-121.
7. Nie, J., et al., *Establishment and validation of a pseudovirus neutralization assay for SARS-CoV-2.* Emerg Microbes Infect, 2020. 9(1): p. 680-686.
8. Watanabe, Y., et al., *Site-specific glycan analysis of the SARS-CoV-2 spike.* Science, 2020. 369(6501): p. 330-333.
9. Hoffmann, M., et al., *SARS-CoV-2 Cell Entry Depends on ACE2 and TMPRSS2 and Is Blocked by a Clinically Proven Protease Inhibitor.* Cell, 2020. 181(2): p. 271-280 e8.
10. Yang, R., et al., *Development and effectiveness of Pseudotyped SARS-CoV-2 system as determined by neutralizing efficiency and entry inhibition test in vitro.* Biosaf Health, 2020.

11. Huang, Y., et al., *Structural and functional properties of SARS-CoV-2 spike protein: potential antivirus drug development for COVID-19.* Acta Pharmacol Sin, 2020. 41(9): p. 1141-1149.

12. Chu, H., et al., *Comparative tropism, replication kinetics, and cell damage profiling of SARS-CoV-2 and SARS-CoV with implications for clinical manifestations, transmissibility, and laboratory studies of COVID-19: an observational study.* The Lancet Microbe, 2020. 1(1): p. e14-e23.

13. Takayama, K., *In Vitro and Animal Models for SARS-CoV-2 research.* Trends Pharmacol Sci, 2020. 41(8): p. 513-517.

14. L. Casey Chosewood, D.E.W., *Biosafety in Microbiological and Biomedical Laboratories*, U.S.D.o.H.a.H. Services, et al., Editors. 2009.

15. Crawford, K.H.D., et al., *Protocol and Reagents for Pseudotyping Lentiviral Particles with SARS-CoV-2 Spike Protein for Neutralization Assays.* Viruses, 2020. 12(5)2020 05 06.

16. Matsuyama, S., et al., *Enhanced isolation of SARS-CoV-2 by TMPRSS2-expressing cells.* Proc Natl Acad Sci U S A, 2020. 117(13): p. 7001-7003.

17. Sarzotti-Kelsoe, M., et al., *Optimization and validation of the TZM-bl assay for standardized assessments of neutralizing antibodies against HIV-1.* J Immunol Methods, 2014. 409: p. 131-146.

18. Easterhoff, D., et al., *Enhancement of HIV-1 infectivity by simple, self-assembling modular peptides.* Biophys J, 2011. 100(5): p. 1325-1334.

19. Ng, K.W., et al., 2020.

20. Calado, M., et al., *Coreceptor usage by HIV-1 and HIV-2 primary isolates: the relevance of CCR8 chemokine receptor as an alternative coreceptor.* Virology, 2010. 408(2): p. 174-182.

21. Nomaguchi, M., et al., *Generation of rhesus macaque-tropic HIV-1 clones that are resistant to major anti-HIV-1 restriction factors.* J Virol, 2013. 87(21): p. 11447-11461.

22. Zhang, X., et al., *Inhibitory effect of human TRIM5α on HIV-1 production.* Microbes and Infection, 2010. 12(10): p. 768-777.

23. Al-Allaf, F.A., et al., *Remarkable stability of an instability-prone lentiviral vector plasmid in Escherichia coli Stbl3.* 3 Biotech, 2013. 3(1): p. 61-70.

24. Cronin, J., X.-Y. Zhang, and J. Reiser, *Altering the tropism of lentiviral vectors through pseudotyping.* Current gene therapy, 2005. 5(4): p. 387-398.

25. Chen, B.K., et al., *Distinct modes of human immunodeficiency virus type 1 proviral latency revealed by superinfection of nonproductively infected cell lines with recombinant luciferase-encoding viruses.* J Virol, 1994. 68(2): p. 654-660.

26. Ishida, Y., et al., *Generation of a neutralization-resistant CCR5 tropic simian/human immunodeficiency virus (SHIV-MK38) molecular clone, a derivative of SHIV-89.6.* J Gen Virol, 2016. 97(5): p. 1249-1260.

27. Matsuda, K., et al., *In vivo analysis of a new R5 tropic SHIV generated from the highly pathogenic SHIV-KS661, a derivative of SHIV-89.6.* Virology, 2010. 399(1): p. 134-143.

28. Seaman, M.S., et al., *Tiered categorization of a diverse panel of HIV-1 Env pseudoviruses for assessment of neutralizing antibodies.* J Virol, 2010. 84(3): p. 1439-1452.

29. Platt, E.J., et al., *Evidence that ecotropic murine leukemia virus contamination in TZM-bl cells does not affect the outcome of neutralizing antibody assays with human immunodeficiency virus type 1.* J Virol, 2009. 83(16): p. 8289-8292.

3.8. Figures

Figure 1.

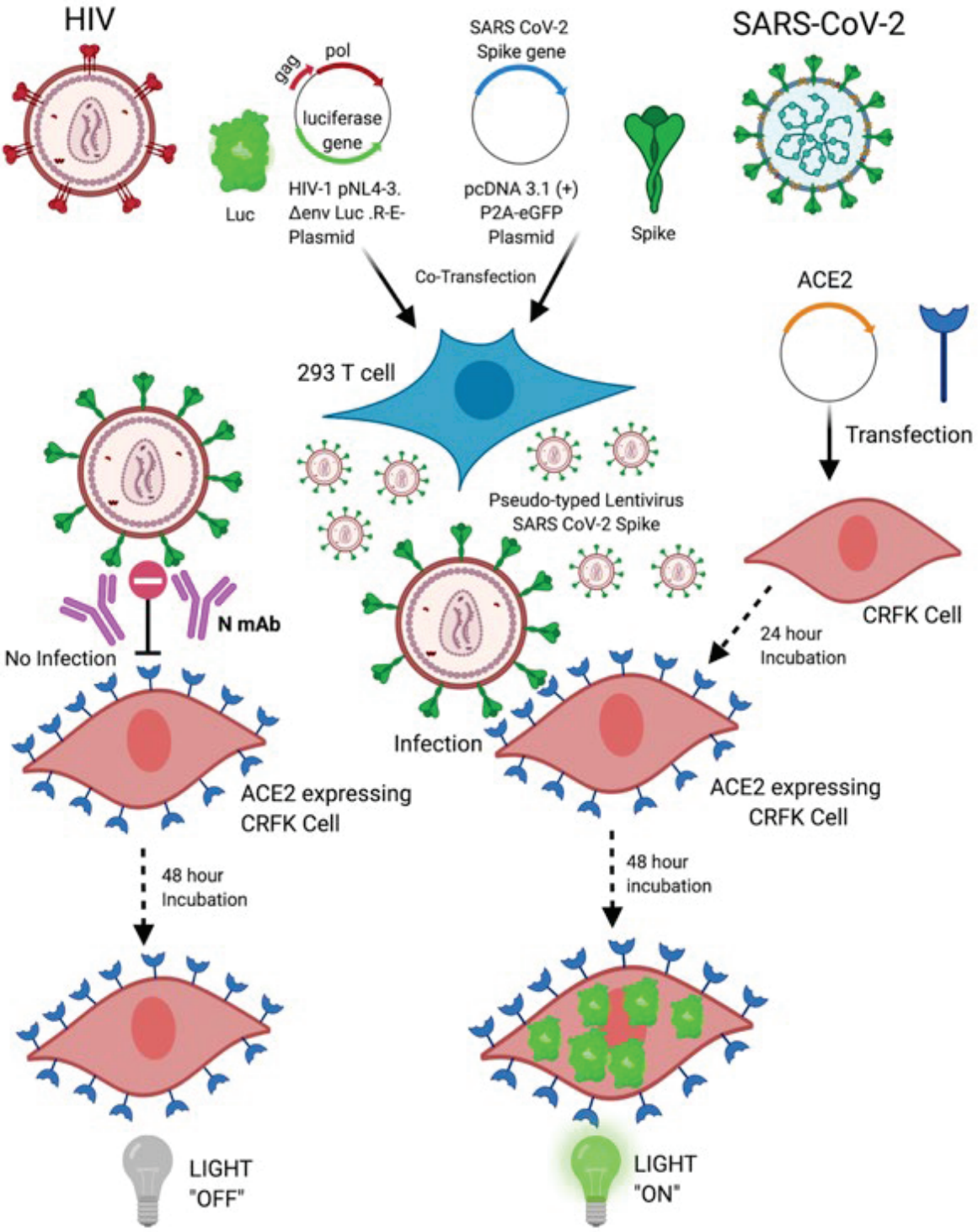

Generation of a pseudo-typed lentivirus coated with SARS-CoV-2 Spike protein using HEK293T cells, and illustration of the neutralization assay principle using ACE2-expressing CRFK cells.

The pseudo-typed lentivirus coated with SARS-CoV-2 Spike (LpVspike[+]) and harbouring the 2019-nCov_pcDNA3.1(+)-P2A-eGFP plasmid was prepared by co-transfecting 5×10^5 cell mL^{-1} of HEK293T cells with the HIV-1 NL4-3 ΔEnv ΔVpr Luciferase Reporter Vector. Transfected HEK293T cells were incubated at 37 °C under 5 % CO_2 for 2 days. The supernatant medium containing LpVspike(+) was harvested and filtered through a 0.45-µm pore size filter. To generate ACE2-expressing cell lines, cells were transfected with pcDNA3.1+/C-(K) DYK-ACE2 and incubated at 37 °C under 5 % CO_2 for 1 day. The transfected cells were then able to transiently express the ACE2 receptor on their membrane surface and could hence be infected by LpVspike(+). Approximately 2.3×10^4 ACE2-expressing cells were infected per well in 96-well plates, and luciferase expression was measured at 48 h post-infection.

Figure 2.

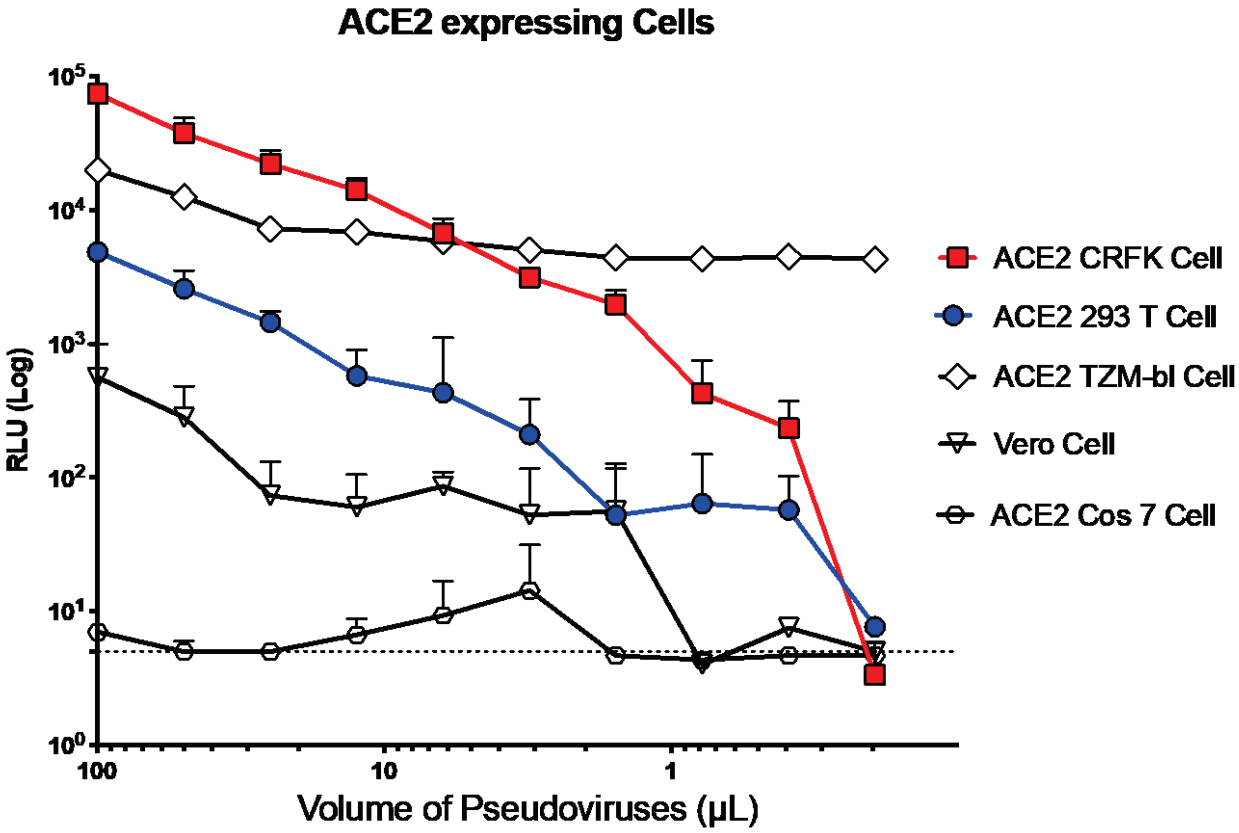

Titres of the LpVspike(+) were determined by measuring relative luciferase units (RLU) at 48 h after infection. Approximately 2.3×10^4 ACE2-expressing cells were seeded per well in 96-well plates. Cells were infected with 100 µL of undiluted LpVspike(+), then two-fold dilutions were made.

Figure 3.

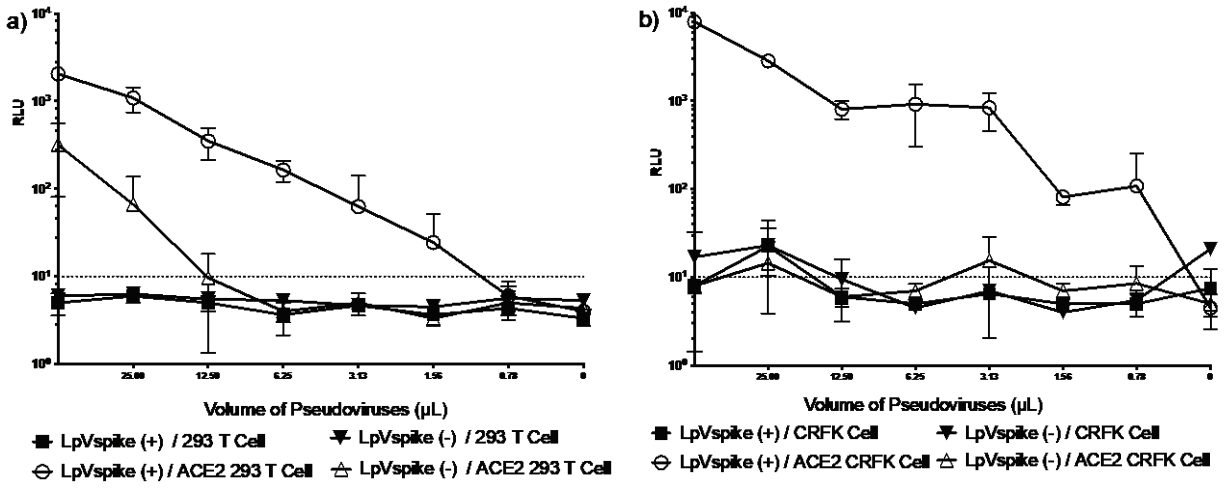

Titres of LpVspike(+) and LpVspike(−) as determined by measuring relative luciferase units (RLU) at 48 h after infection. Cells at concentrations of approximately 2.3×10^4 cell of each cell line (HEK293T, ACE2-expressing HEK293T, CRFK and ACE2-expressing CRFK) were seeded per well in 96-well plates. The initial volume of LpVspike(+) used for infection was 50 µL of undiluted virus, then three 1:2 dilutions were made.

Figure 4.

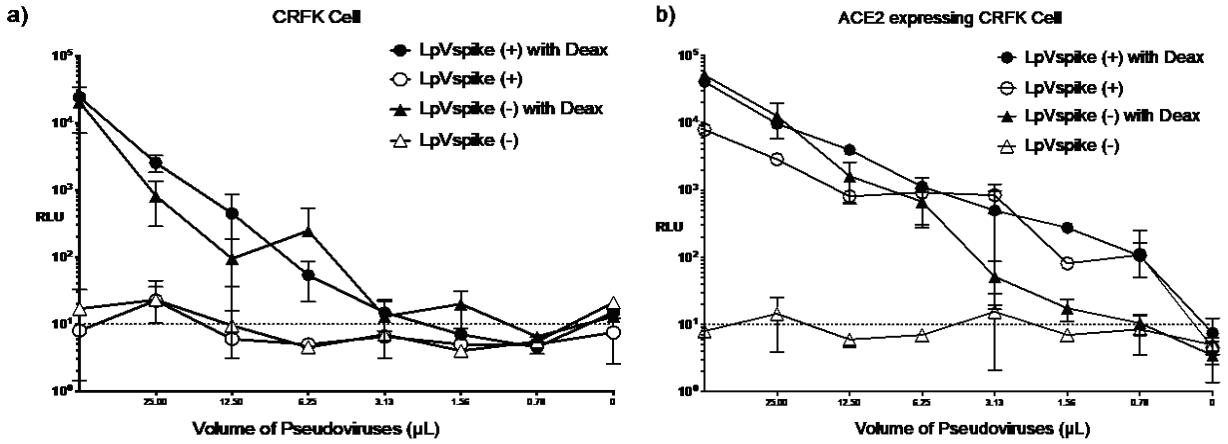

Relative luciferase unit (RLU) measurements were taken at 48 h after infection. Approximately 2.3×10^4 cells of each cell line (CRFK and ACE2-expressing CRFK) were seeded per well in 96-well plates. The initial volume of LpVspike(+) used for infection was 50 µL of undiluted virus, then three 1:2 dilutions were made. Dextran (Deax) was added to the medium to a final concentration of 8 µg mL^{-1}.

Figure 5.

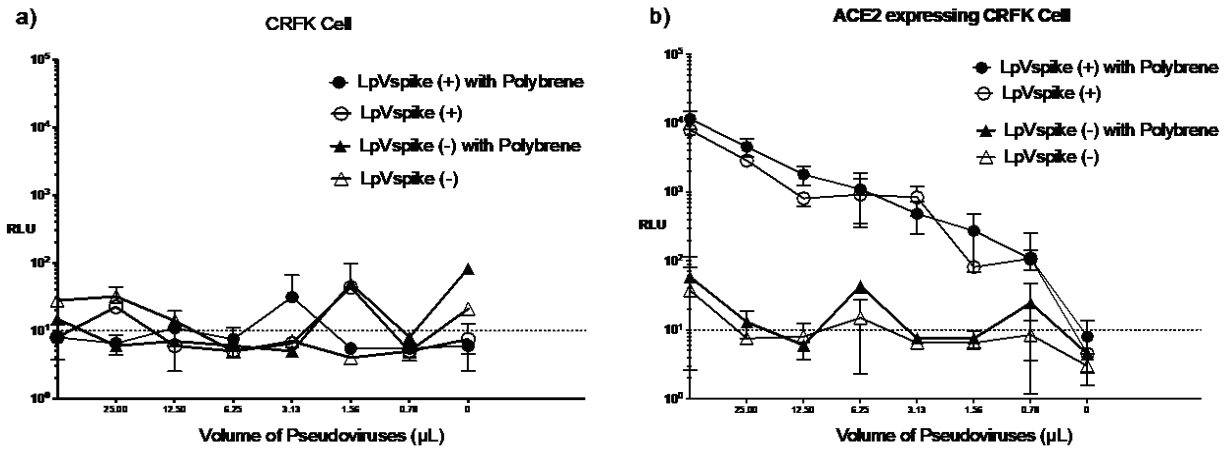

Relative luciferase unit (RLU) measurements were taken at 48 h after infection. Approximately 2.3×10^4 cells of each cell line (CRFK and ACE2-expressing CRFK) were seeded per well in 96-well plates. The initial volume of LpVspike(+) used for infection was 50 µL of undiluted virus, then three 1:2 dilutions were made. Polybrene was added to the medium to a final concentration of 10 µg mL^{-1}.

Figure 6.

(a) (b)

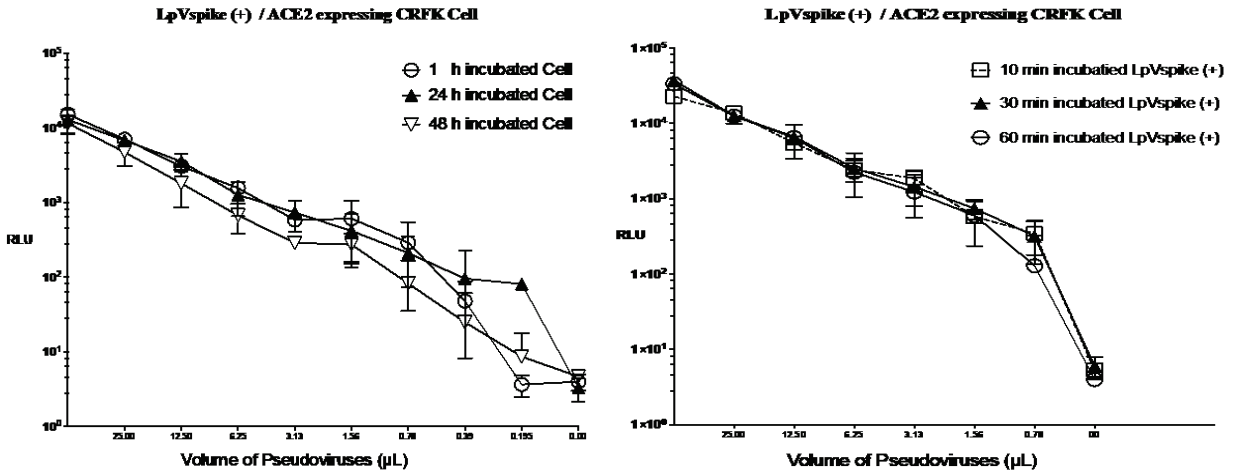

(a) Effect of varying the incubation period following ACE2 transfection on LpVspike(+) infectivity. Open circles: infectivity of CRFK cells at 1 h after ACE2 transfection. Black triangles: infectivity of CRFK cells at 24 h after ACE2 transfection. Open inverted triangles: infectivity of CRFK cells at 48 h after ACE2 transfection. The initial volume of LpVspike(+) used for infection was 50 µL of undiluted virus, then three 1:2 dilutions were made. Approximately 2.3×10^4 ACE2-expressing CRFK cells were seeded per well in 96-well plates. Relative luciferase unit (RLU) measurements were taken at 48 h after infection. (b) Effect of varying the viral incubation period at 37 °C on LpVspike (+) infectivity. Following infection, cells were incubated with the virus for 10 min (open squares), 30 min (black triangles) or 60 min (open circles). The initial volume of LpVspike(+) used for infection was 50 µL of undiluted virus, then three 1:2 dilutions were made. Approximately 2.3×10^4 ACE2-expressing CRFK cells were seeded per well in 96-well plates. RLU measurements were taken at 48 h after infection.

Figure 7.

(a) (b)

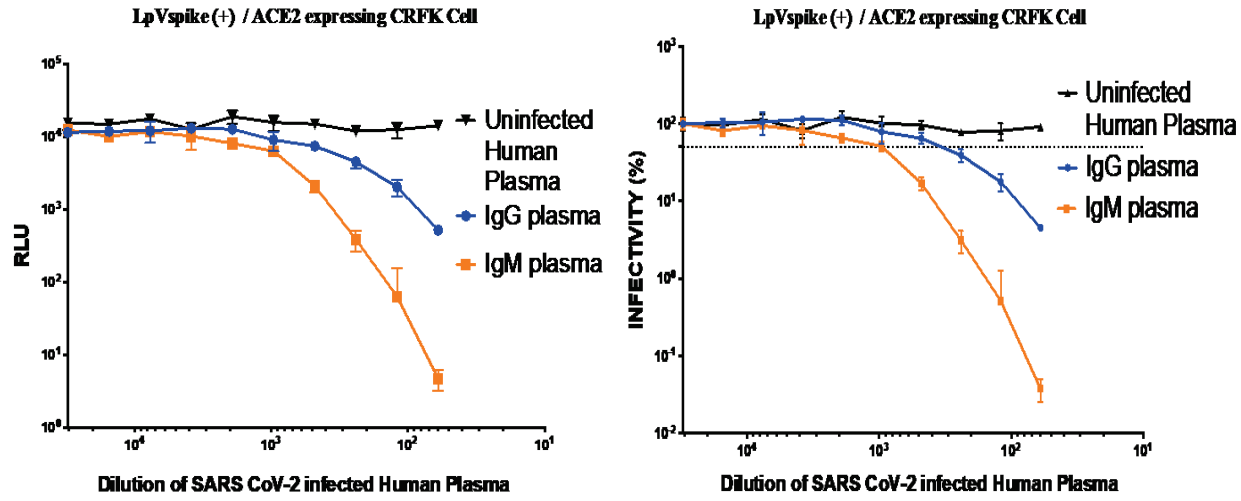

Neutralization of LpVspike(+) with human plasma extracted from patients infected with SARS-CoV-2. After pre-incubating 100 TCID50 of LpVspike(+) with human plasma, the virus-plasma mixture was added to ACE2-expressing CRFK cells and incubated at 37 °C for 48 h, after which luciferase activity was measured. Plasma was subjected to serial two-fold dilutions from an initial dilution of 1:60 down to 1:15,360 (X axis). X axis and Y axis are indicated with log scale. Left figure show row data, right figure is calculated by left figure.

Figure 8.

(a) (b)

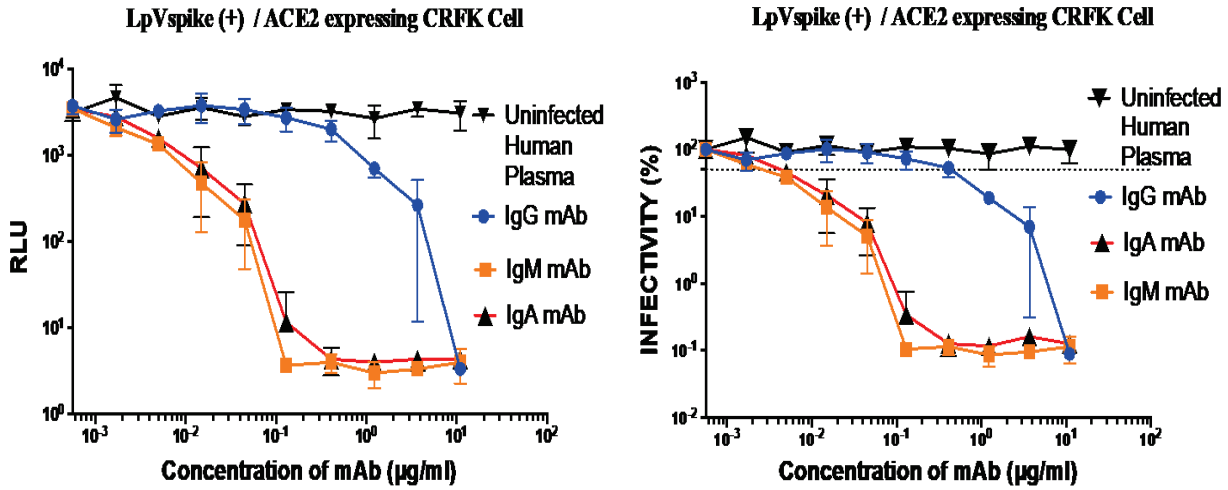

Neutralization of LpVspike(+) with anti-SARS-CoV-2 monoclonal antibodies (mAbs). After pre-incubating 100 TCID50 of LpVspike(+) with each anti-SARS-CoV-2 neutralizing mAb, the mAb-virus mixtures were added to ACE2-expressing CRFK cells and cultured for 48 h, after which luciferase activity was measured. The IgG, IgM and IgA mAbs were subjected to serial three-fold dilutions, from an initial concentration of 10 μg mL^{-1} down to 0.016 μg mL^{-1}. X axis and Y axis are indicated with log scale. Left figure show row RLU data, right figure is calculated by left figure.

Chapter 4.

General Discussion

4.1. Discussion

In this thesis, to deepen our understanding of neutralizing mechanism by antibody, I described two important worldwide spreading viral pathogens, HIV and SARS CoV-2.

In chapter 2, I focused on the neutralization resistance and genetic mutations of HIV-1 envelope protein using SHIV model. Since HIV-1 evades antibody reaction rapidly by changing antigenicity, it provides a good example to investigate relation between the antigenicity and protein structure depending on amino acid charges and N-Glycans [1]. In this study, I suggested that increase of negative charge at the V1V2 region of the envelope protein changes its conformation to bury immunodominant V3 region inside stably, making the envelope protein resistant to KD247 monoclonal antibody whose epitope is present on the apex of the V3 area (Chapter 2- Figure 8). The alteration on the electrostatic potential of viral protein structure could also impact infectivity beyond its antigenicity. There is a study that the positive charge of the spike protein of SARS-CoV-2 might increase binding ability against the negatively charged region of the ACE2 receptor [2, 3]. Therefore, to develop our understanding of electrostatic potential charging on protein structure of viruses will help us fighting viral pathogens.

In chapter 3, I described the relationship between the function and structure of neutralizing antibodies, developing a novel system that contains a pseudo-typed lentivirus coated with the SARS-CoV-2 spike protein and ACE2-transfected cat CRFK cells as the host cell line. While IgG has two antigen binding sites (Ag-bs), dimeric IgA has four Ag-bs. A pentameric IgM molecule has 10 Ag-bs and can bind 10 small antigens. However, due to steric restrictions, only five large antigen molecules can be bound by one IgM molecule [4]. According to this theory while IgG binds only one large antigen (virion), dimeric and pentameric IgA and IgM can bind multiple virions (Chapter 4, Figure 1). My results that show much more efficient neutralization of pseudo-

typed SARS CoV-2 by IgM and IgA form possessing the same Fab than the IgG form (Chapter 3, Figure 8) can be explained by the capacity of IgM and IgA that can bind multiple virions. Moreover, these results suggest the novel way to generate potent antibody medicines that efficiently neutralize SARS-CoV-2.

Lastly, I hope my results will provide new insight into understanding antigen-antibody reaction, helping developing new measures fighting infectious diseases.

4.2. Reference

1. Harada, S. and K. Yoshimura, *Driving HIV-1 into a Vulnerable Corner by Taking Advantage of Viral Adaptation and Evolution.* Front Microbiol, 2017. **8**: p. 390.
2. Hassanzadeh, K., et al., *Considerations around the SARS-CoV-2 Spike Protein with Particular Attention to COVID-19 Brain Infection and Neurological Symptoms.* ACS Chem Neurosci, 2020. **11**(15): p. 2361-2369.
3. Hou, Y.J., et al., *SARS-CoV-2 D614G variant exhibits efficient replication ex vivo and transmission in vivo.* Science, 2020: p. eabe8499.
4. Nezlin, R., *CHAPTER 1 - General Characteristics of Immunoglobulin Molecules*, in *The Immunoglobulins*, R. Nezlin, Editor. 1998, Academic Press: New York. p. 3-73.

4.3. Figure 1.

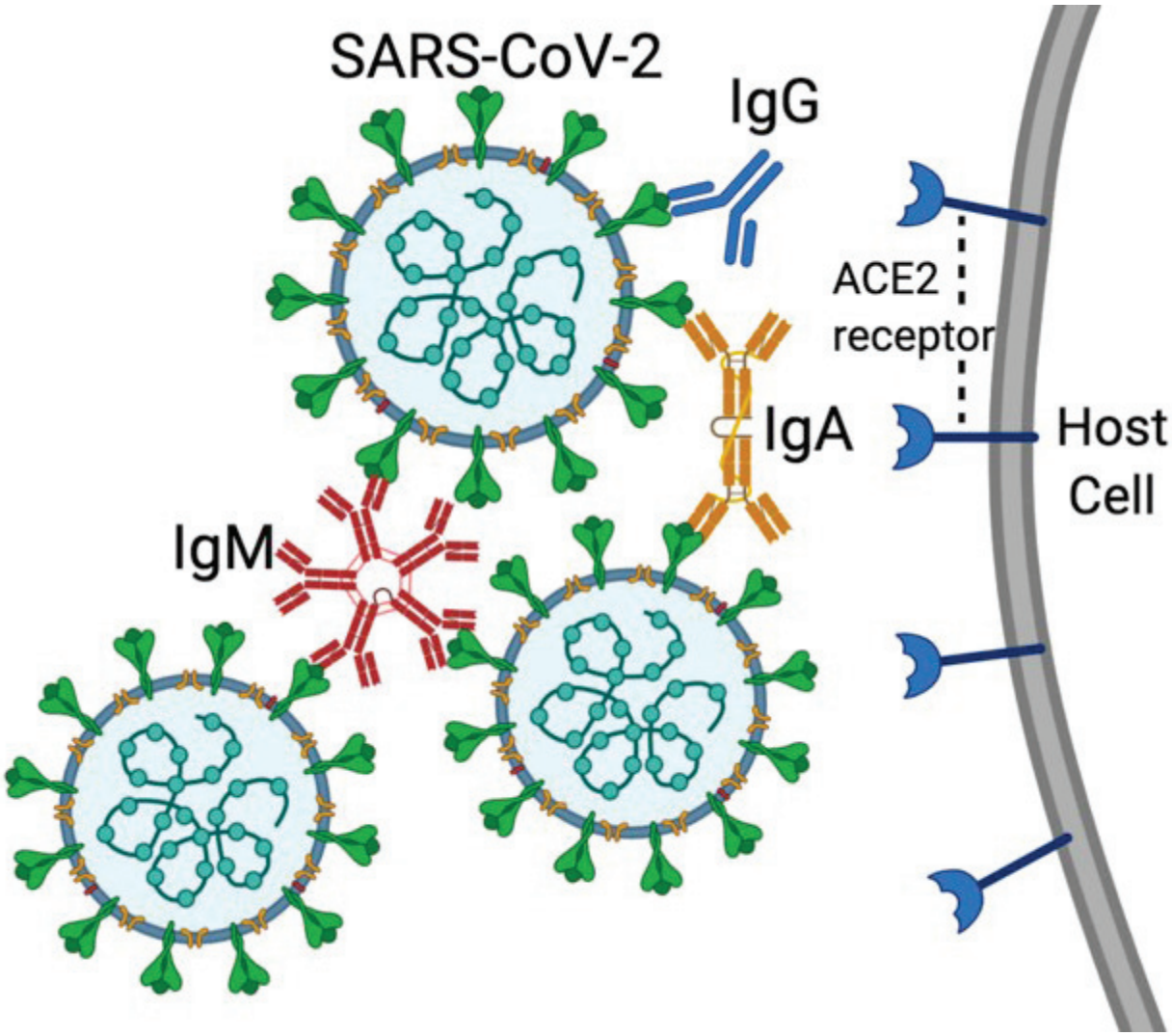

Three anti-SARS-CoV-2 neutralizing mAbs including IgG, IgM and IgA can neutralize SARS-CoV-2. IgG has 2 antigen binding site (Ag bs), dimeric IgA has 4 Ag bs. A pentameric IgM molecule has 10-antigen combining sites and can bind 10 small antigens. However, due to steric restrictions, only five large viral antigens can be bound by one IgM molecule, IgG is also bind only one large antigen; dimeric, trimeric and pentameric IgA can bind more than 1 large antigens.

Acknowledgements.

I’m incredibly grateful to my supervisor, Tomoyuki Miura, to allow me to study in his laboratory and provide valuable comments and continued supports to all my research life. I also thank generous Hisatoshi Shida who always supports and motivates me scientifically, Zafer Yazici who guided me to start my scientific career in Japan and Komatsu Tadahiko, Oda Tamihei, Yuki Nakamura and Soner Ulusoy for comments and assistance during the study. I also thank Emad Ahmadi, Yoshida Atsushi, Otsuki Mai, Yuna Abe, Matsuura Kanako and Emre Unal to share their feedbacks kindly about my research. Also, I am thankful to the Kyoto Turkish Association members, the office members of Graduate School of Human and Environmental Studies, the Residences of Yoshidaryou Dormitory and Nakamura Family to show me behaved like a family. Finally, I would like to thank to my family.

※　著作権等

Pathogens 2020,9, 181; doi:10.3390/pathogens9030181